Cell Reports

Article

Chaperone-mediated autophagy in neuronal dendrites utilizes activity-dependent lysosomal exocytosis for protein disposal

Graphical abstract

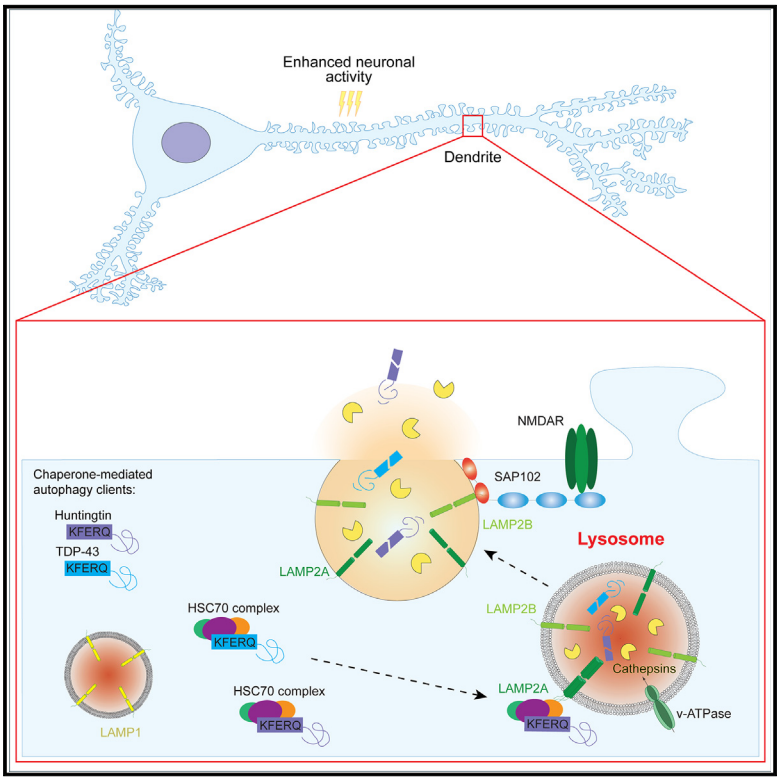

Highlights

- LAMP1 and LAMP2B mark different dendritic vesicular populations
- NMDAR activity induces fusion of LAMP2B-positive lysosomes with the plasma membrane
- LAMP2B/LAMP2A lysosomes are competent for CMA
- Lysosomal fusion leads to the extracellular release of CMA clients

Authors

Katarzyna M. Grochowska, Marit Sperveslage, Rajeev Raman, ..., Laura Laprell, Boris Fehse, Michael R. Kreutz

Correspondence

katarzyna.grochowska@zmnh.uni-hamburg.de (K.M.G.), michael.kreutz@zmnh.uni-hamburg.de (M.R.K.)

In brief

Grochowska et al. show that a subpopulation of dendritic lysosomes positive for lysosomal proteins LAMP2B and LAMP2A fuses with the plasma membrane upon activation of NMDA receptors. Activity-dependent fusion leads to the release of supersaturated, disease-relevant dendritic proteins huntingtin and TDP-43.

Grochowska et al., 2023, Cell Reports *42*, 112998
August 29, 2023
https://doi.org/10.1016/j.celrep.2023.112998

CellPress

Cell Reports

CellPress
OPEN ACCESS

Article

Chaperone-mediated autophagy in neuronal dendrites utilizes activity-dependent lysosomal exocytosis for protein disposal

Katarzyna M. Grochowska,[1,2,8,*] Marit Sperveslage,[1,2,8] Rajeev Raman,[2] Antonio V. Failla,[3] Dawid Głów,[4] Christian Schulze,[5] Laura Laprell,[5] Boris Fehse,[4] and Michael R. Kreutz[1,2,6,7,9,*]

[1]Leibniz Group "Dendritic Organelles and Synaptic Function," Center for Molecular Neurobiology, ZMNH, University Medical Center Hamburg-Eppendorf, 20251 Hamburg, Germany
[2]Research Group Neuroplasticity, Leibniz Institute for Neurobiology, 39118 Magdeburg, Germany
[3]UKE Microscopic Imaging Facility (umif), University Medical Center Eppendorf, 20251 Hamburg, Germany
[4]Research Department Cell and Gene Therapy, Department of Stem Cell Transplantation, University Medical Centre Hamburg-Eppendorf (UKE), 20246 Hamburg, Germany
[5]Institute of Synaptic Physiology, Center for Molecular Neurobiology, ZMNH, University Medical Center Hamburg-Eppendorf, 20251 Hamburg, Germany
[6]Center for Behavioral Brain Sciences, Otto von Guericke University, 39120 Magdeburg, Germany
[7]German Center for Neurodegenerative Diseases (DZNE), 39120 Magdeburg, Germany
[8]These authors contributed equally
[9]Lead contact
*Correspondence: katarzyna.grochowska@zmnh.uni-hamburg.de (K.M.G.), michael.kreutz@zmnh.uni-hamburg.de (M.R.K.)
https://doi.org/10.1016/j.celrep.2023.112998

SUMMARY

The complex morphology of neurons poses a challenge for proteostasis because the majority of lysosomal degradation machinery is present in the cell soma. In recent years, however, mature lysosomes were identified in dendrites, and a fraction of those appear to fuse with the plasma membrane and release their content to the extracellular space. Here, we report that dendritic lysosomes are heterogeneous in their composition and that only those containing lysosome-associated membrane protein (LAMP) 2A and 2B fuse with the membrane and exhibit activity-dependent motility. Exocytotic lysosomes dock in close proximity to GluN2B-containing N-methyl-D-aspartate-receptors (NMDAR) via an association of LAMP2B to the membrane-associated guanylate kinase family member SAP102/Dlg3. NMDAR-activation decreases lysosome motility and promotes membrane fusion. We find that chaperone-mediated autophagy is a supplier of content that is released to the extracellular space via lysosome exocytosis. This mechanism enables local disposal of aggregation-prone proteins like TDP-43 and huntingtin.

INTRODUCTION

The extreme length of cellular processes constitutes a major challenge for neuronal proteostasis.[1,2] As yet, little is known on how neurons accomplish local protein degradation. Lysosomes are heterogeneous acidic organelles that serve as a degradative endpoint for late endosomes and autophagosomes.[3–6] Conflicting reports suggest that distal dendrites are either devoid of mature lysosomes[7,8] or that catabolically active lysosomes are present,[9–11] indirectly suggesting that cargo might be degraded locally. Interestingly, trafficking and motility of these lysosomes appears to be regulated by activation of glutamate receptors[9] and reportedly they exhibit activity-regulated fusion with the plasma membrane.[10] The functional implications of this activity-dependent regulation are currently to a large extent elusive, and the knowledge about dendritic lysosomal exocytosis as such is scarce. It reportedly depends upon the release of Ca^{2+} stored in the lysosomal lumen, which results in steep Ca^{2+} increase and precedes SNARE-dependent fusion with the plasma membrane.[10] In functional terms, released cathepsin B might then activate matrix metalloprotease 9, which in turn can lead to remodeling of the extracellular matrix (ECM) and subsequent dendritic spine growth.[10]

However, if dendritic lysosomal exocytosis indeed exists it is still unclear how lysosomal fusion sites are defined, whether all lysosomes in dendrites can be primed for fusion, and whether release-competent lysosomes serve a specific need. Lysosomal biogenesis depends upon a gradual delivery of lysosomal components to endosomes and autophagosomes,[3–5] a process that will result in heterogeneous populations of vesicles with different stages of maturation. A systematic analysis of lysosomal subpopulations in dendrites is currently lacking, but ultimately necessary since in axons such an analysis has revealed the absence of mature lysosomes despite the presence of LAMP proteins.[12,13] Moreover, lysosomes are not only a catabolic endpoint of endosomal and autophagy pathways they play a

well-documented role in chaperone-mediated autophagy (CMA).[14–17] About 30% of soluble proteins contain a CMA motif[14,18] that is recognized by the chaperone Hsc70.[19,20] Hsc70 delivers the cargo to the organelle surface for subsequent translocation to the lysosomal lumen via the CMA receptor lysosome-associated membrane protein (LAMP) 2A.[16,20–22] In neurons, CMA is involved in axonal proteostasis[16,23,24] but it has not been investigated yet in dendrites.

Using an array of imaging and biochemical techniques, we identified in this study different dendritic lysosomal subpopulations, characterized the molecular composition of exocytic lysosomes and the mechanisms for their docking and fusion, and addressed their role in local N-methyl-D-aspartate-receptor (NMDAR)-regulated protein disposal. Most important we show that lysosomal exocytosis results in release of CMA clients to the extracellular space.

RESULTS

LAMP1 and LAMP2 do not label the same dendritic lysosome pool

Lysosomes exhibit a highly dynamic exchange of membrane and a heterogeneous molecular composition that might be overlooked with immunocytochemical staining using only one lysosomal marker.[2] The most frequently used lysosomal markers for immunocytochemistry and cellular imaging are LAMP1 and LAMP2.[2] When we performed confocal imaging of segments from proximal and distal dendrites of hippocampal primary neurons and labeled lysosomes with corresponding antibodies we observed that, on average, less than 40% of both proteins indeed colocalized (Figures 1A and 1B). shRNA protein knockdown or CRISPR-Cas9 gene deletion documented the specificity of both antibodies for immunocytochemical applications in primary neurons (Figures S1A–S1D). Further evidence that lysosomes of different composition might exist in dendrites came from live imaging experiments where we expressed both proteins with an mKate fluorescent tag in hippocampal neurons (Figures 1C and 1D). Three isoforms of LAMP2 exist, termed 2A-C, which differ mainly in their cytoplasmic tail[25,26] and from which LAMP2C is expressed at low levels in neurons.[26,27] We found that 80% of LAMP2B-mKate vesicles associate with LAMP2A and vice versa 60% of LAMP2A with LAMP2B (Figures S1E–S1G), indicating that in dendrites a larger fraction of lysosomes will express both proteins.

Interestingly, when we next looked at organelle motility, we observed that LAMP1-mKate vesicles in dendrites are clearly less mobile than those expressing LAMP2B-mKate irrespective of their distance to the soma (Figures 1C and 1D), suggesting that lysosomal trafficking might be differentially regulated. We next used BODIPY-pepstatin A, a cell-permeable cathepsin D-binding fluorescent compound to specifically label the active protease in the lumen of mature lysosomes.[28] Live imaging revealed that approximately 70% of either LAMP1- or LAMP2B-positive vesicles contain active proteases (Figures 1E, 1F, and S1H–S1J). Collectively, these data point to differences in trafficking and molecular composition of dendritic lysosomes and this indirectly suggests that they might execute different functions.

LAMP2-positive lysosomes dock in proximity to GluN2B-containing NMDAR

It was reported previously that lysosome trafficking and exocytosis might be regulated by neuronal activity,[9,10] but it is unclear whether specific signaling events are involved. NMDAR, especially those containing the GluN2B subunit, are present at synaptic (spine and shaft synapses) but also at extrasynaptic sites.[29,30] Immunocytochemical analysis with antibodies directed against the postsynaptic scaffold protein Shank3, the presynaptic marker protein Bassoon, and the GluN2B subunit of NMDARs revealed that in hippocampal primary neurons at DIV16 roughly 65% of GluN2B immunofluorescence puncta localize to synaptic sites, out of which around 30% were associated with shaft synapses and 70% with spine synapses (Figure S2A–S2C). Thus, around 35% of surface-expressed GluN2B localized to extrasynaptic sites present in the dendritic shaft (Figure S2B).

We next addressed whether NMDAR activity regulates motility and positioning of LAMP2-positive lysosomes. To this end, we performed live imaging using total internal reflection fluorescence microscopy (TIRFM) to exclusively image lysosomes directly below the plasma membrane. Mature hippocampal neurons (DIV16) were transfected with LAMP2B-mKate and the GluN2B NMDAR subunit fused to superecliptic pHluorin (SEP), a pH-dependent tag exclusively labeling receptors inserted in the plasma membrane[31] (Figures 2A–2E, S2D, and S2E). We observed that 34% of SEP-GluN2B transiently associates with LAMP2B-mKate (Figures 2A–2C). The average duration of each event lasted around 1 min (Figure 2E). Furthermore, approximately 40% of SEP-GluN2B was observed in proximity to LAMP2B-mKate and vice versa (Figures 2C and 2D).

To further corroborate these findings, we performed live imaging of neurons transfected with SEP-GluN2B and incubated with Magic Red, a fluorescent dye labeling catabolically active cathepsin B in mature lysosomes[32] (Figures 2F–2J). The fraction of Magic Red-positive puncta found in proximity to SEP-GluN2B (around 40%) (Figures 2H–2J) was comparable with those of LAMP2B-mKate (Figures 2C–2E).

NMDAR activation stalls LAMP2B-positive lysosomes and induces their fusion with the plasma membrane

When we next stimulated neurons with 20 μM NMDA we observed that LAMP2B-mKate motility was reduced within 6 min (Figures 2K–2M; Video S1). A similar effect was observed for Magic Red-positive vesicles (Figures 2N–2P), which suggests that NMDAR activity influences motility of mature lysosomes close to the plasma membrane. No stalling was observed for peroxisomes (Figure S2F–H) or for LAMP1-positive vesicles (Figures 2Q–2S), which further suggests that a distinct dendritic LAMP2B-positive lysosome pool exists whose motility is regulated by NMDAR activity.

We next investigated whether neuronal activity induced by field stimulation results in membrane fusion of the LAMP2-positive lysosome pool and whether this fusion occurs in a GluN2B-dependent manner. To this end, we used TIRFM to show regions of the cell membrane and a LAMP2B construct with a SEP tag in the luminal domain (Figures 3, S3A, and S3B). We indeed observed a gradual increase in SEP-associated fluorescence intensity following field stimulation compared with baseline

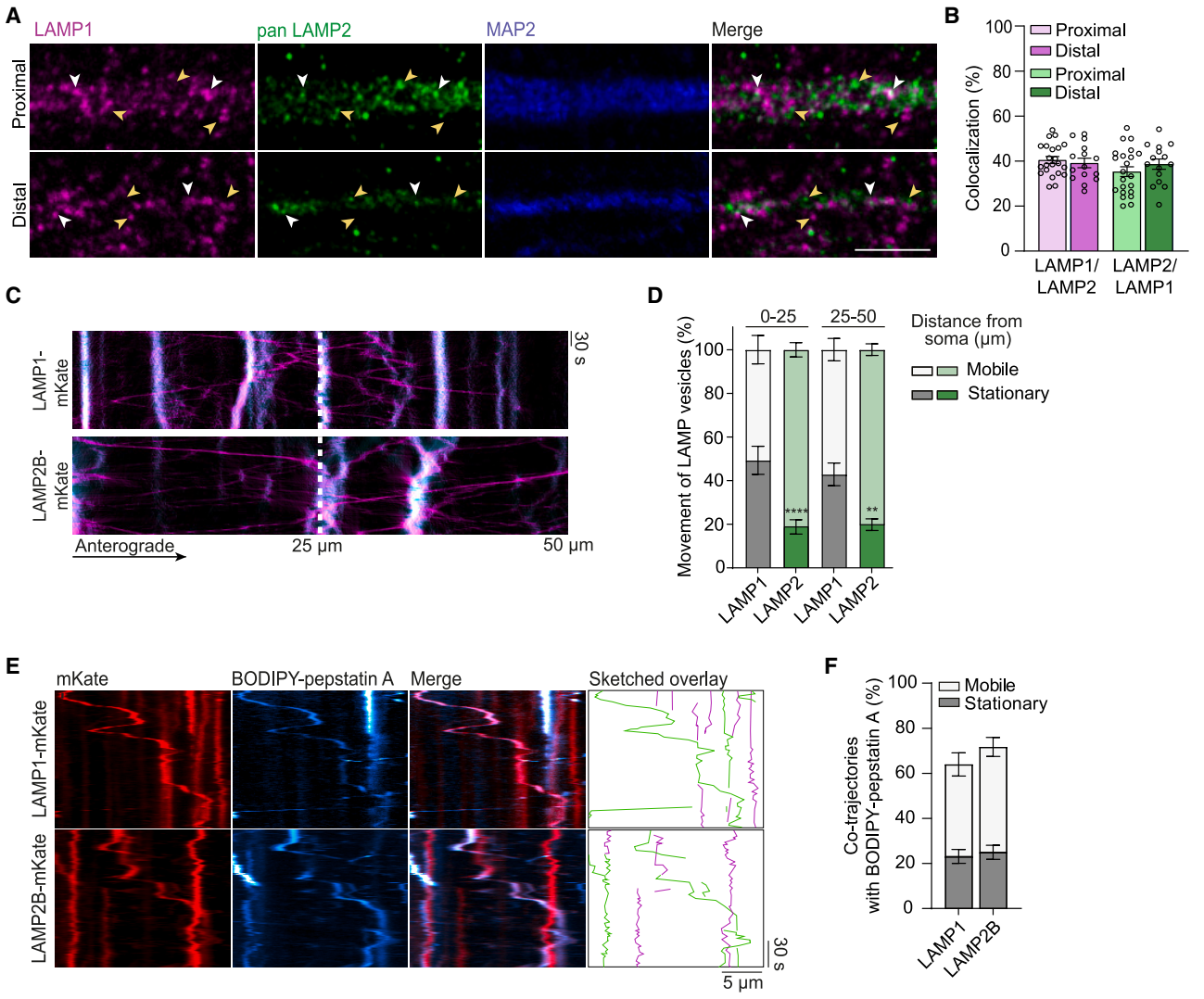

Figure 1. LAMP1 and LAMP2 are found in different dendritic lysosomal pools

(A) Representative confocal images of proximal and distal dendrites from DIV16 cultured hippocampal neurons immunostained against LAMP1 (magenta), pan LAMP2 (green), and MAP2 (blue). Scale bar, 5 µm. White arrows indicate overlapping and orange arrows indicate non-overlapping signal.

(B) Quantification of colocalization between LAMP1 and LAMP2 in proximal and distal dendrites. Around 40% of LAMP1 and LAMP2 colocalize in both distal and proximal segments. n = 15–23 cells from 4 independent cultures.

(C and D) Motility of LAMP1-mKate- and LAMP2B-mKate-positive organelles respective to the distance to the soma. (C) Kymographs show stationary traces (magenta) and mobile vesicles (cyan). (D) LAMP2B-mKate has higher mobility as compared with LAMP1-mKate. n = 31–43 dendritic segments, 14–27 cells from 5 independent cultures. Ns; $p > 0.999$ for distance factor and ****$p < 0.0001$ for LAMP factor by two-way ANOVA with post hoc Tukey test.

(E) A major fraction of LAMP1-mKate or LAMP2B-mKate overlap with BODIPY-pepstatin A. Sketched overlay depicts vesicles positive (green) and negative (magenta) for BODIPY-pepstatin A, labeling the active lysosomal enzyme CatD.

(F) Quantification of LAMP1-mKate and LAMP2B-mKate trajectories positive and negative for BODIPY-pepstatin A. n = 17–19 cells from 3 independent cultures.

(B, D, and F) Data are plotted as average ± SEM.

conditions (Figures 3A–3D). Both the increase in fluorescence as well as the fusion density were decreased upon pre-incubation with the GluN2B antagonist ifenprodil (Figures 3A–3D). Most importantly, we did not observe fusion of SEP-tagged LAMP1 (Figures S3C–S3F), further indicating that LAMP2- and LAMP1-positive lysosomes are functionally distinct.

Similar to field stimulation, bath application of NMDA in hippocampal primary neurons enhanced fusion of SEP-LAMP2B vesicles (Figures 3E–3H) with a steep increase in SEP-LAMP2B fluorescence intensity in response to stimulation (Figures 3E–3G). Ifenprodil decreased the number of fusion events and fusion fluorescence intensity (Figures 3E–3H). We next addressed whether fusion occurs in proximity to GluN2B-containing NMDAR. To measure the distance between the fusion region and SEP-GluN2B, we used LAMP2B tagged with pHuji, a red-shifted, pH-sensitive dye (Figure S3G).[33] We found a median

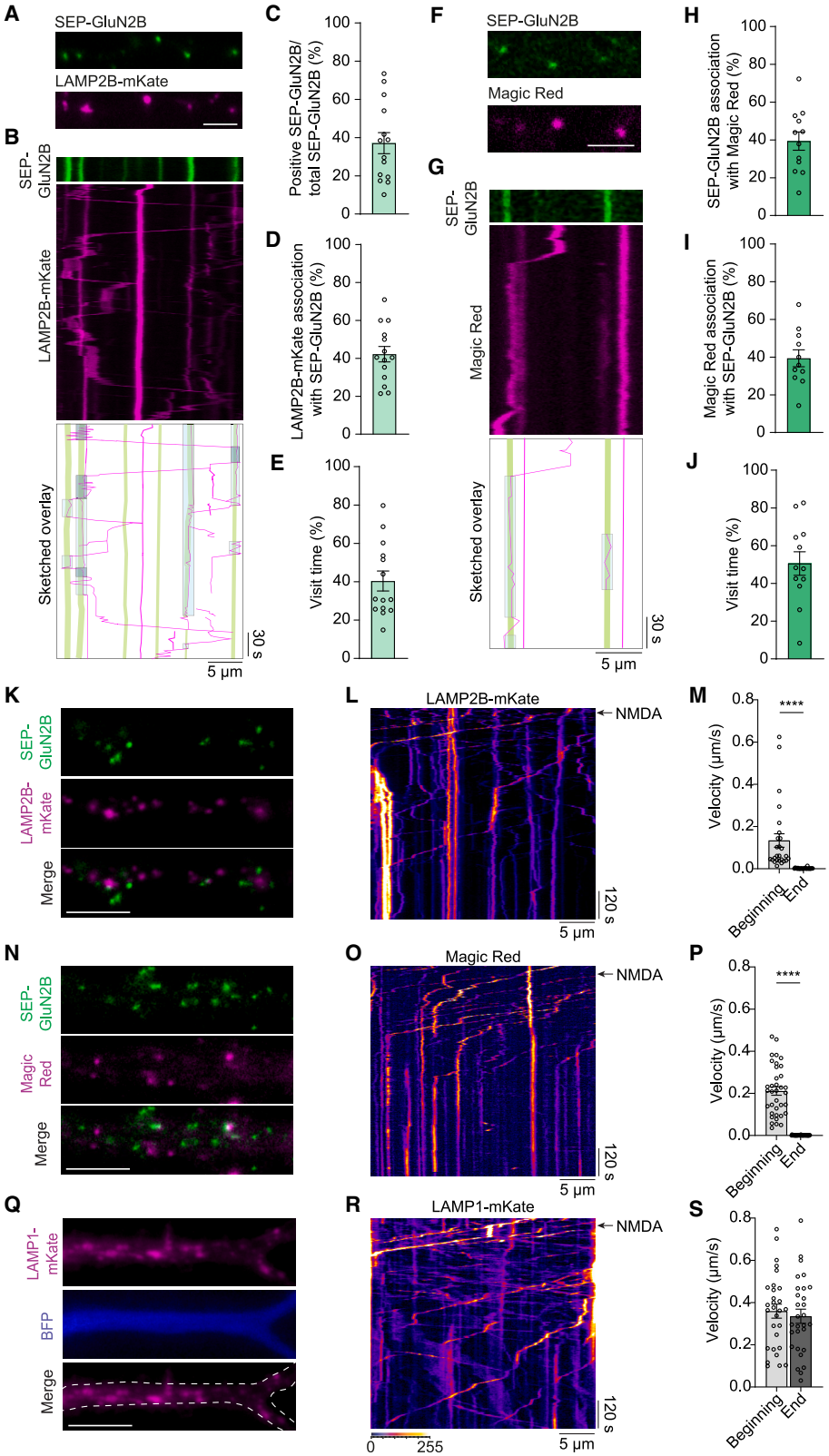

(legend on next page)

distance between fusion spots to GluN2B of 0.17 μm, indicating a tight spatial association (Figures S3G–S3H).

To finally prove a causal relationship between GluN2B activation and lysosome fusion we used a genetic approach utilizing primary neurons from a CRISPR-Cas9 knockin mouse, which overexpress Cas9 protein and GFP reporter protein. Expression of a plasmid encoding a gRNA directed against GluN2B resulted in a significant reduction of surface expressed GluN2B (Figures S3I and S3J). Most important, in neurons transfected with gRNA targeting GluN2B we observed clearly decreased fusion density as well as fluorescence intensity compared with control neurons (Figures S3K–S3N).

LAMP2-positive lysosomes associate with SAP102/Dlg3 in close proximity to GluN2B-containing NMDAR

What might be the underlying mechanism for docking and fusion of LAMP2B-positive lysosomes in proximity to GluN2B-containing NMDAR? In heterologous co-immunoprecipitation experiments we found no evidence for a direct association of LAMP2B with the cytoplasmic tail of GluN2B, while a positive control, the synapto-nuclear-protein messenger Jacob, showed binding to this region as shown previously (Figures S4A and S4B).[34,35] Published evidence suggests a functional and physical interaction of GluN2B with the scaffolding protein SAP102/Dlg3 not only in spine synapses but also in the dendritic shaft.[36–39] SAP102/Dlg3 is a member of the membrane-associated guanylate kinases (MAGUK) family and the N terminus of SAP102/Dlg3 contains PDZ domains that associate prominently with a PDZ-binding motif at the C terminus of GluN2B.[37,39] Members of the MAGUK family in general play a role in the subunit-specific regulation of NMDAR trafficking and localization; and, in particular, surface expression depends on the binding of the PDZ ligand to PDZ domains of MAGUKs.[40] In line with published work we found extensive colocalization of surface-expressed GluN2B and SAP102/Dlg3 in dendrites of hippocampal primary neurons (Figures S4C and S4E). Moreover, we observed that more than 30% of LAMP2B-mKate associates with SAP102/Dlg3 in dendrites of hippocampal neurons (Figures 4A and 4B) and bath application of NMDA significantly increased the association of SAP102/Dlg3 with LAMP2B-mKate even further (Figures 4A and 4B).

We next asked whether the SEP-LAMP2B fusion sites are characterized by the presence of SAP102/Dlg3. In live imaging experiments, the identification of fusion sites relies on the changes of the fluorescence of the pH-sensitive SEP tag, which is quenched in fixed cells.[41] Therefore, we performed live staining on SEP-LAMP2B-expressing neurons with an SEP-detecting nanobody labeled with AF647N, which allows for labeling of recently exocytosed SEP molecules.[41] Subsequently the samples were processed with antibodies detecting SAP102/Dlg3 (Figures 4C–4E). We could observe a significant increase in the nanobody fluorescent signal upon NMDA stimulation (Figures 4C and 4D). Furthermore, 80% of the fusion signal was associated with SAP102/Dlg3 (Figures 5C and 5E). Taken together, these data suggest that lysosomal fusion predominantly occurs in close proximity of SAP102/Dlg3-positive puncta along the dendritic plasma membrane.

SAP102/Dlg3 directly interacts with LAMP2B, and this interaction is crucial for stalling and fusion of lysosomes

We therefore next wondered whether stalling of LAMP2B in close proximity to GluN2B might be mediated by a physical interaction with SAP102/Dlg3. Pull-down experiments with the bacterially produced cytoplasmic tail of LAMP2B fused to a His-SUMO tag provided proof for a direct interaction with the GFP-tagged SH3-GK domain of SAP102/Dlg3, but not the N-terminal PDZ domains containing part (Figures 4F–4H and S4F) or His-SUMO coupled to the resin (Figure 4G). Pull-down experiments with LAMP2A cytoplasmic tail showed no binding between LAMP2A and the SH3-GK domain of SAP102/Dlg3 (Figures 4I and S4G). Furthermore, in HEK293T cells the SH3-GK domain-containing part of SAP102/Dlg3 is recruited to the cytosolic part of LAMP2B when this short stretch of amino acids is targeted to Golgi membranes (Figure S4H) in a Golgi-tracker assay.[42] No recruitment was seen for the PDZ domain-containing part of SAP102/Dlg3, although recruitment was observed when the C terminus of GluN2B containing the PDZ ligand was targeted to the Golgi as positive control (Figure S4H).

To study the functional relevance of the interaction of SAP102/Dlg3 and LAMP2B we designed a dominant-negative TAT peptide carrying the sequence of the LAMP2B cytoplasmic tail.[25]

Figure 2. LAMP2B-positive lysosomes stall after NMDA stimulation

(A) Representative images of hippocampal neurons (DIV14–17) transfected with SEP-GluN2B (green) and LAMP2B-mKate (magenta). Scale bar, 5 μm.

(B) Kymographs of LAMP2B-mKate and SEP-GluN2B. Blue-shaded sketched trajectories represent transient association between LAMP2B-mKate (magenta) at SEP-GluN2B (green).

(C) Quantification of the percentage of SEP-GluN2B visited by LAMP2B-mKate.

(D) Visit time of LAMP2B-mKate at SEP-GluN2B normalized to the total acquisition time.

(E) Percentage of LAMP2B-mKate that associates with SEP-GluN2B. n = 8–12 cells from 2 to 7 independent cultures.

(F) SEP-GluN2B-transfected neurons were incubated with Magic Red to label lysosomes with active CatB. Scale bar, 5 μm.

(G) Kymographs of Magic Red and SEP-GluN2B. Blue-shaded sketched trajectories represent transient association between Magic Red (magenta) at SEP-GluN2B (green).

(H and I) (H) Fraction of SEP-GluN2B associating with Magic Red or (I) Magic Red associating with SEP-GluN2B.

(J) Visit times of Magic Red-positive vesicles at SEP-GluN2B. n = 7–12 dendritic segments from 5 independent cultures.

(K–S) Velocity of LAMP2B-mKate-positive vesicles in dendrites of DIV14–16 neurons decreases upon application of 20 μM NMDA. (N–P) Velocity of Magic Red-positive vesicles in dendrites of DIV14–16 neurons decreases upon application of 20 μM NMDA. (Q–S) Velocity of LAMP1-mKate-positive vesicles in dendrites of DIV14–16 neurons does not change upon application of 20 μM NMDA. (K and N) Representative images of SEP-GluN2B-transfected neurons together with (K) LAMP2B-mKate or (N) incubated with Magic Red. (Q) LAMP1-mKate was co-transfected with BFP to visualize the cell outline. Scale bar, 5 μm. (L, O, and R) Representative kymographs. Arrow indicates the time point of bath application of NMDA. (M, P, and S) Scatter bar plots representing velocity at the beginning and the end of the stream. ****$p < 0.0001$ by two-tailed Mann-Whitney U test. n = 4–14 cells from 5 independent cultures. (L, O, and R) Lookup table indicates the pixel intensities from 0 to 255. (C–E, H–J, M, P, and S) Data are plotted as average ±SEM.

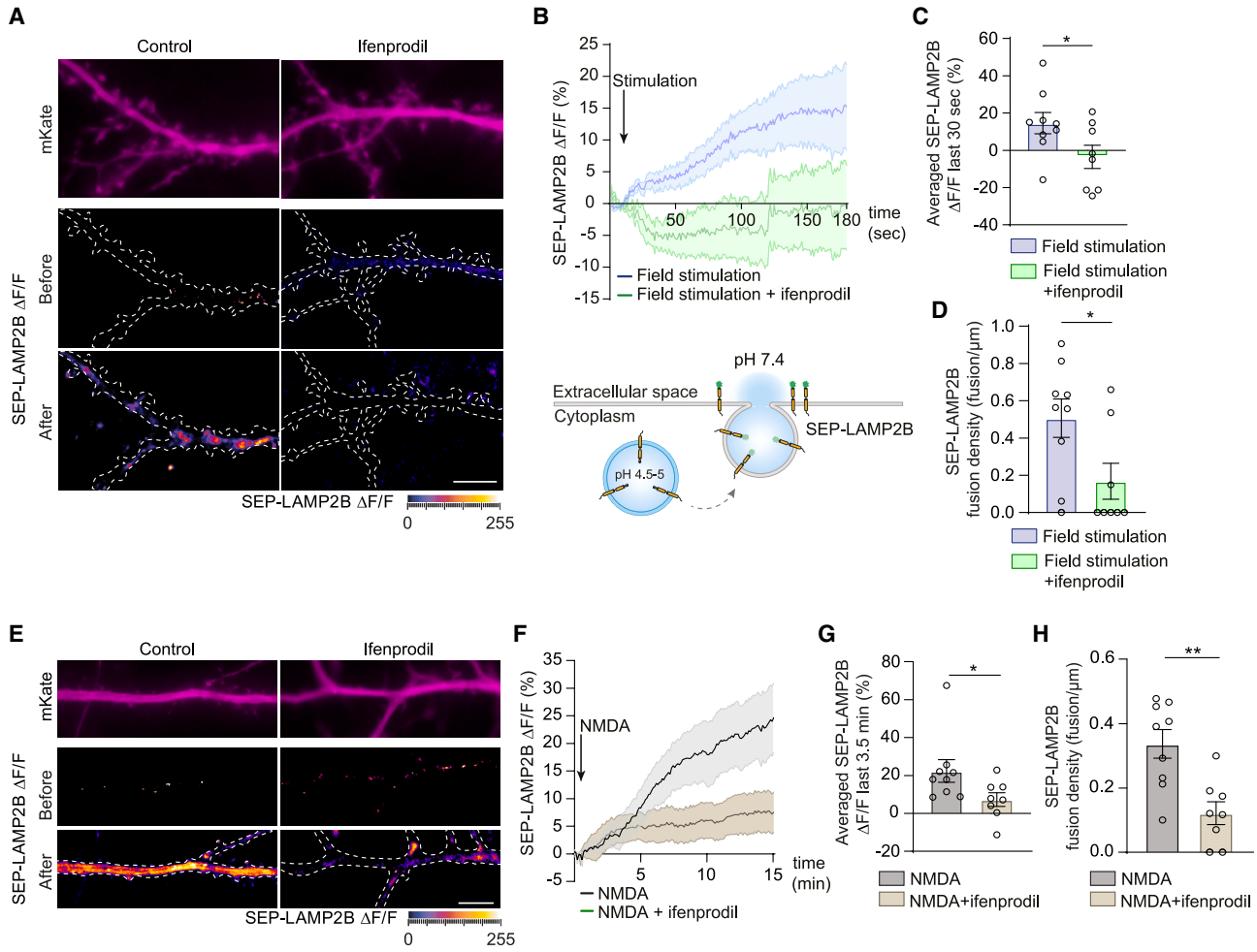

Figure 3. NMDARs control LAMP2B fusion with the plasma membrane

(A) TIRFM images of hippocampal neurons (DIV16) transfected with SEP-LAMP2B (depicted as ΔF/F; before, averaged baseline frames: after, averaged last 20 frames of the stream) and mKate as volume fill. Field stimulation results in an increase of the SEP fluorescence, which is significantly decreased in the presence of ifenprodil. Scale bar, 10 μm.

(B) Top: averaged change in fluorescence over time post stimulation normalized to baseline. Shading indicates ± SEM. Below: scheme of SEP-LAMP2B—fluorescence is quenched in acidic pH and increased upon fusion with the plasma membrane.

(C and D) Ifenprodil reduces both (C) the averaged SEP-LAMP2B fluorescence intensity from last 30 s and (D) the fusion density. n = 8–9 cells from 5 independent experiments. *$p < 0.05$ by two-tailed unpaired Student's t test.

(E) TIRFM images of hippocampal neurons (DIV16) transfected with mKate as volume fill and SEP-LAMP2B (depicted as ΔF/F; before, averaged baseline frames; after, averaged last 20 frames of the stream). Bath application of NMDA induces SEP-LAMP2B fusion. Scale bar, 10 μm.

(F) Averaged change in fluorescence over time post stimulation normalized to baseline. Shading indicates ±SEM.

(G and H) Treatment with ifenprodil decreases (G) averaged fusion intensity (last 3.5 min) and (H) fusion density. n = 8–9 cells from 6 independent cell cultures. *$p < 0.05$ by (G) two-tailed unpaired Student's t test or (H) **$p < 0.01$ by two-tailed Mann-Whitney U test. (A and E) Lookup table indicates the pixel intensities from 0 to 255. (B–D and F–H) Data are plotted as average ±SEM.

This TAT peptide disrupted binding to SAP102/Dlg3 in pull-down assays (Figure 4J). We therefore next administered this peptide or the corresponding scrambled control to hippocampal cultures and assessed the motility of LAMP2B-mKate upon stimulation with NMDA (Figures 2, 4K, and 4L). In contrast to the scrambled peptide (Figures 4K and 4L) or non-treated cells (Figure 2K–2M) we did not observe stalling of LAMP2B-mKate in neurons treated with the TAT-LAMP2B-404–415 peptide (Figures 4K and 4L). In addition, blockage of the interaction between the SH3-GK domain of SAP102/Dlg3 and the LAMP2B cytoplasmic tail strongly reduced fusion of pHuji-LAMP2B with the plasma membrane (Figures 4M–4P).

The central role of SAP102/Dlg3 in stopping and fusion of lysosomes was additionally confirmed by experiments in Cas9-expressing neurons transfected with a construct encoding gRNA targeting SAP102/Dlg3 that showed reduced SAP102/Dlg3 expression (Figures S4I and S4J). In these neurons, the motility of catabolically active lysosomes was assessed with the use of the pepstatin A-based SiR-lysosome dye, which binds to active cathepsin D.[43] In support of the important role of SAP102/Dlg3

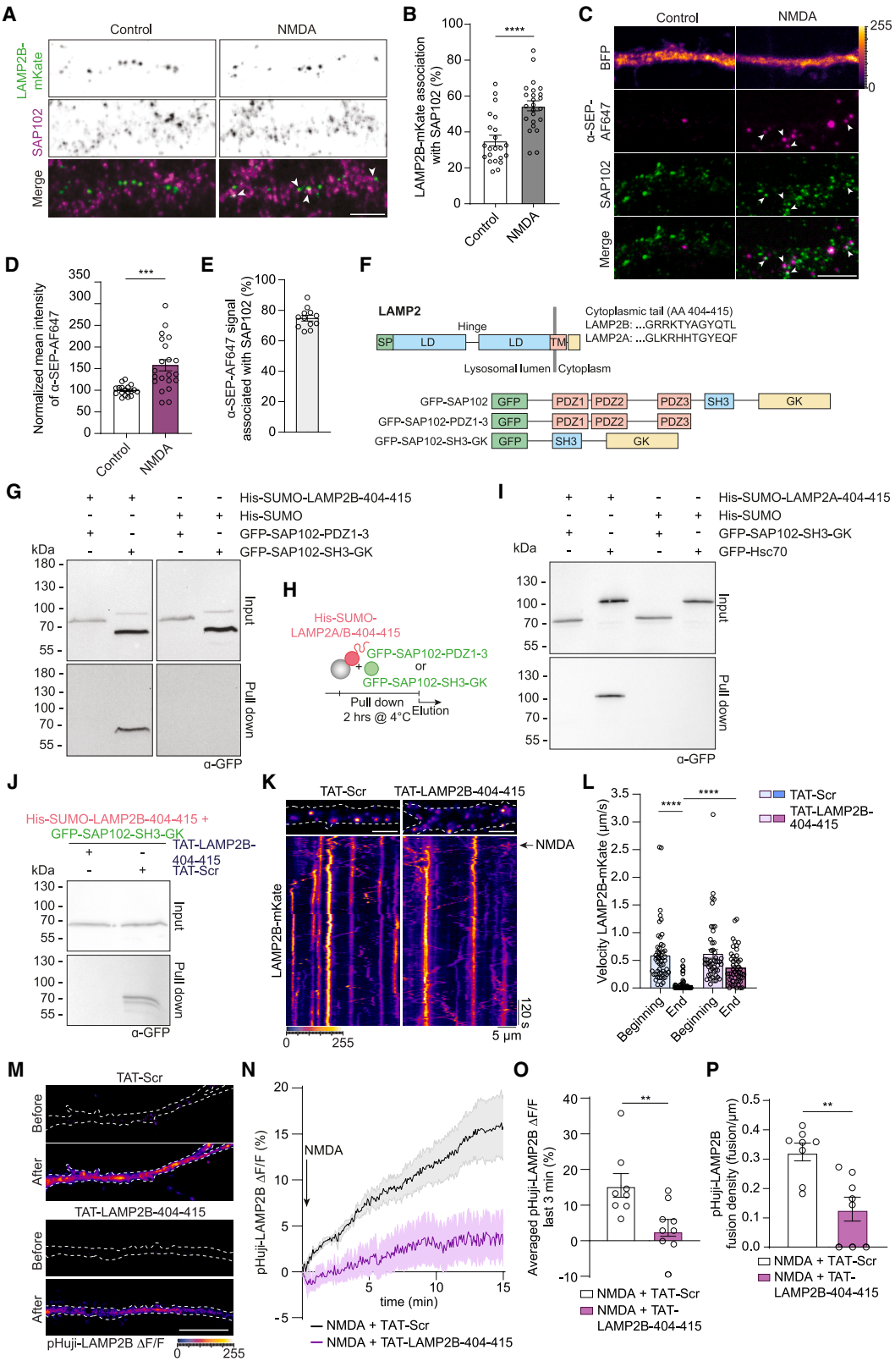

(legend on next page)

for docking of LAMP2B-containing vesicles, we observed no stopping of catabolically active lysosomes upon bath application of NMDA in these experiments (Figures S4K and S4L).

Exocytotic lysosomes in dendrites incorporate chaperone-mediated autophagy clients

Collectively the experiments outlined above suggest that LAMP2-positive lysosomes dock to SAP102/Dlg3 and thereby associate with GluN2B-containing NMDAR complexes and that this docking is regulated by GluN2B activity and essential for lysosomal fusion. Exocytosis of lysosomes is reportedly accompanied by release of cathepsins and potentially a digestion of the ECM that results in spine growth.[10] When we determined changes in spine morphology 30–45 min following bath application of picrotoxin in organotypic hippocampal slices we indeed observed an increase of dendritic spine size for spines located within 5 μm of the center of lysosome fusion (Figure S5A–S5C). This increase could not be observed for slices perfused with vehicle (Figure S5A–S5C), where no fusion was observed (Figure S5C).

However, it is unclear whether spine growth is merely an inevitable consequence and side effect of lysosomal release of cathepsins or whether this is the major function of lysosome exocytosis. We, therefore, addressed in the final set of experiments the question how this fusion relates to protein degradation. Lysosomes are reportedly involved in CMA, a Hsc70 chaperone-dependent process where a specific CMA-targeting motif (KFERQ) of the substrate is recognized by the chaperone.[14,16,19,20,22] The subsequent delivery to the lysosomal surface, unfolding, and translocation into the lumen is mediated by the association of Hsc70 with multimerized LAMP2A.[22,44,45] Interestingly, stimulated emission depletion (STED) super-resolution microscopy revealed that Hsc70 localizes in the lumen and on the membrane of LAMP2B-GFP-positive lysosomes (Figures 5A–5D).

A widely used tool to monitor cellular CMA activity is a CMA sensor where the KFERQ motif is fused to a fluorescent protein.[17,19,46] In the next set of experiments, we transfected hippocampal neurons with tRFP-KFERQ and LAMP2B-GFP and stained with an antibody recognizing LAMP2A. We compared baseline conditions with cells treated with 20 μM NMDA or 20 μM CA77.1, a potent CMA activator, as positive control.[17,47] Expectedly, we found a significantly increased number of tRFP-KFERQ dendritic puncta (Figure S6A) and increased association with LAMP2A/B-positive lysosomes following treatment with CA77.1 (Figures 5E and 5F). Interestingly, this increase and the rapid association with lysosomal membranes was also seen upon 15 min of treatment with 20 μM NMDA (Figures 5E, 5F, and S6A).

Disposal of CMA clients to the extracellular space occurs via lysosomal exocytosis

Taken together, these data raise the possibility that exocytosis of dendritic LAMP2A/B-containing lysosomes contributes to an activity-dependent removal of aggregation-prone proteins. To test this hypothesis, we used TAR DNA-binding protein 43 (TDP-43), a well-established CMA substrate.[48] We expressed TDP-43 tagged with HA-tdTomato[49] together with LAMP2B-GFP in primary neurons and, with STED super-resolution microscopy, we observed that TDP-43-tdTomato is indeed prominently targeted to the LAMP2B-positive lysosomal lumen in dendrites (Figures 6A–6C). Moreover, endogenous TDP-43 was present in LAMP2-positive lysosomes, as evidenced by antibody-based immunocytochemical staining and subsequent STED imaging and by the Pearson's colocalization coefficient (Figures 6D–6G). Moreover, we could also observe some overlap of TDP-43

Figure 4. Stalling and fusion of LAMP2B-positive lysosomes depends on direct interaction of LAMP2B and the SH3-GK domain of SAP102

(A) Representative confocal images of dendrites from hippocampal neurons expressing LAMP2B-mKate and stained for endogenous SAP102. Arrowheads indicate colocalization. Scale bar, 5 μm.

(B) Scatter bar plots representing percentage of LAMP2B-mKate-positive lysosomes associated with SAP102 revealed increased colocalization in NMDA-treated neurons. n = 22–24 neurons from 3 independent cultures. ****$p < 0.0001$ by two-tailed unpaired Student's t test.

(C–E) LAMP2B fusion spots labeled with α-SEP-AF647 significantly associate with SAP102. (C) Representative confocal images of hippocampal neurons transfected with BFP and SEP-LAMP2B, co-stained with SAP102//Dlg3 antibody and α-SEP-AF647. White arrowheads indicate colocalization between SEP-LAMP2B and SAP102. Scale bar, 5 μm. (D) Averaged fluorescence intensity of SEP-detecting nanobody. n = 18–21 neurons from 3 independent cell cultures. ***$p < 0.01$ by two-tailed unpaired Student's t test. (E) Percentage of LAMP2B fusion spots associating with SAP102. n = 11 dendritic stretches from 3 independent cell cultures.

(F) Scheme representing the different domains of SAP102 and LAMP2B/A.

(G–I) The cytoplasmic tail of (G) LAMP2B but not (I) LAMP2A binds directly to the SH3-GK domain of SAP102. (G) Pull-down assay performed with immobilized His-SUMO-LAMP2B-404-415 or His-SUMO and lysate from COS-7 cells overexpressing the respective GFP-SAP102 constructs. (H) The cytoplasmic tail of LAMP2A/B (AA 404-415) fused to His-SUMO is used for the pull-down assay together with GFP-tagged SAP102 constructs.

(I) No interaction was detected in pull-down experiments between His-SUMO-LAMP2A-404-415 and the SH3-GK domain of the scaffold protein SAP102.

(J) TAT-LAMP2B-404-415 disrupts binding between LAMP2B (AA 404-415) and the SH3-GK domain of SAP102. The interaction between His-SUMO-LAMP2B-404-415 and GFP-SAP102-SH3-GK is blocked by incubation of TAT-LAMP2B-404-415 but not TAT scrambled (TAT-Scr).

(K and L) TAT-LAMP2B-404-415 peptide impairs NMDA-dependent lysosomal stalling and fusion. (K) Kymographs and representative images from dendritic stretches of hippocampal neurons transfected with LAMP2B-mKate. Arrow indicates NMDA bath application. Scale bar, 5 μm.

(L) The presence of TAT-LAMP2B-404-415 abolishes the decrease of LAMP2B-mKate velocity. n = 9–10 cells from 5 independent cultures. ****$p < 0.0001$ Kruskal-Wallis multiple comparisons test.

(M) Representative dendrites of pHuji-LAMP2B-transfected neurons before and after NMDA stimulation in the presence of TAT-Scr or TAT-LAMP2B-404-415. Scale bar, 10 μm.

(N) Averaged pHuji-LAMP2B intensity normalized to baseline over time ± SEM.

(O and P) Scatter bar plots representing the difference in (O) averaged fluorescence intensity (last 3 min) and (P) fusion density between TAT-LAMP2B-404-415- and TAT-Scr-treated neurons. n = 8 cells from 6 independent cultures **$p < 0.01$ two-tailed unpaired Student's t test. (C, K, and M) Lookup table indicates the pixel intensities from 0 to 255. (B, D, E, L, and N–P) Data are plotted as average ±SEM.

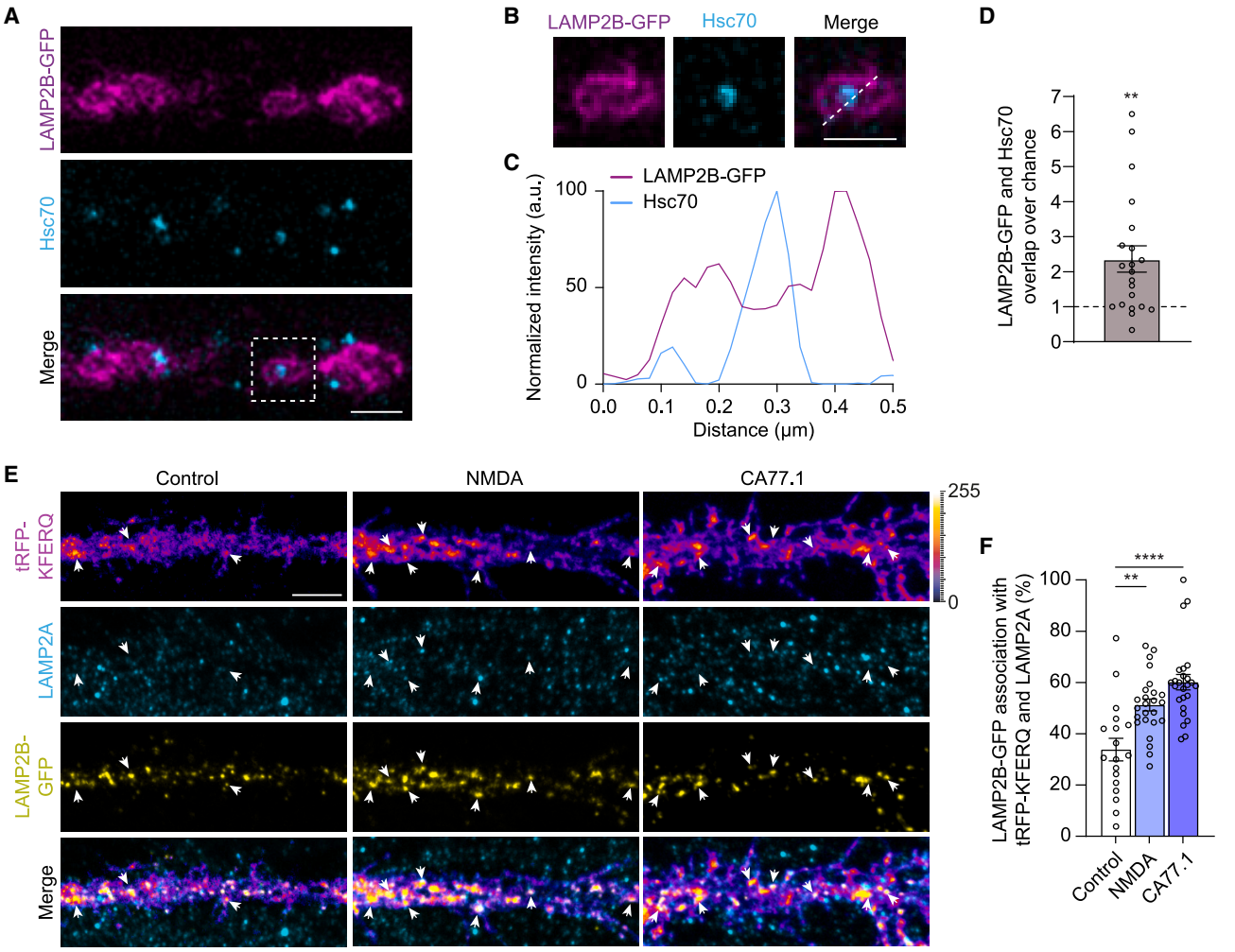

Figure 5. Dendritic LAMP2B and LAMP2A are localized on CMA-competent lysosomes

(A and B) (A) Deconvolved STED images from hippocampal neurons transfected with LAMP2B-GFP and stained against endogenous Hsc70. Scale bar, 500 nm. The dashed square indicates a ROI shown in (B).

(C) Line profiles representing the normalized fluorescence intensity generated from the dashed line depicted in (B). Scale bar, 500 nm.

(D) LAMP2B-GFP signal overlaps with endogenous Hsc70 significantly higher than expected due to chance (overlap with Hsc70 channel rotated by 180°). n = 21 cells from 2 independent cell cultures. **p < 0.01 by one-sample t test. Dotted line indicates overlap expected due to chance.

(E and F) Application of NMDA or CMA activator, CA77.1, induces association of tRFP-KFERQ CMA sensor with LAMP2A/B-positive vesicles. (E) Confocal images of dendritic segments of hippocampal neurons (DIV16) transfected with LAMP2B-GFP, tRFP-KFERQ and stained with antibody against LAMP2A. Arrowheads indicate triple colocalization. Scale bar, 5 μm. (F) Quantification of colocalization of LAMP2B-GFP with tRFP-KFERQ and LAMP2A. ****p < 0.0001, **p < 0.01 by Kruskal-Wallis multiple comparisons test. n = 18–25 cells from at least 3 independent cell cultures. (D) Lookup table indicates the pixel intensities from 0 to 255. (D and F) Data are plotted as average ±SEM.

and Hsc70 immunosignals (Figures 6H–6J). In subsequent live-cell imaging we observed that, in neurons expressing LAMP2B-BFP and TDP-43-tdTomato, more than half of TDP-43 co-trafficked in mature LAMP2B-BFP-positive lysosomes that were visualized by incubation with BODIPY-pepstatin A (Figure 6K–6M; Video S2).

Given that an endogenous CMA client is present in LAMP2B-positive lysosomes we next addressed whether lysosomal release of TDP-43 will occur. We indeed found that TDP-43 is exocytosed from neuronal cells in an activity-dependent manner. When we infected cortical cultures with an AVV9 virus expressing GFP or TDP-43-GFP (Figures S6B and S6C) and stimulated neurons for 15 min with 20 μM NMDA we observed clearly increased TDP-43-GFP content in the supernatant, as measured by GFP-ELISA (Figure 7A). No NMDA-dependent release of overexpressed GFP was detected (Figure 7A).

To corroborate these findings, we next performed dot blot assays following NMDA stimulation (Figures 7B–7F) and tested for the presence of endogenous TDP-43 (Figures 7B and 7C) as well as the classical CMA target GAPDH in the medium (Figures 7B and 7D).[14,45] We could indeed detect an increased release of these proteins to the extracellular space following acute stimulation with 20 μM NMDA for 15 min of cortical cultures (Figures 7B–7D). Of note, this effect is stunning because the levels of proteins

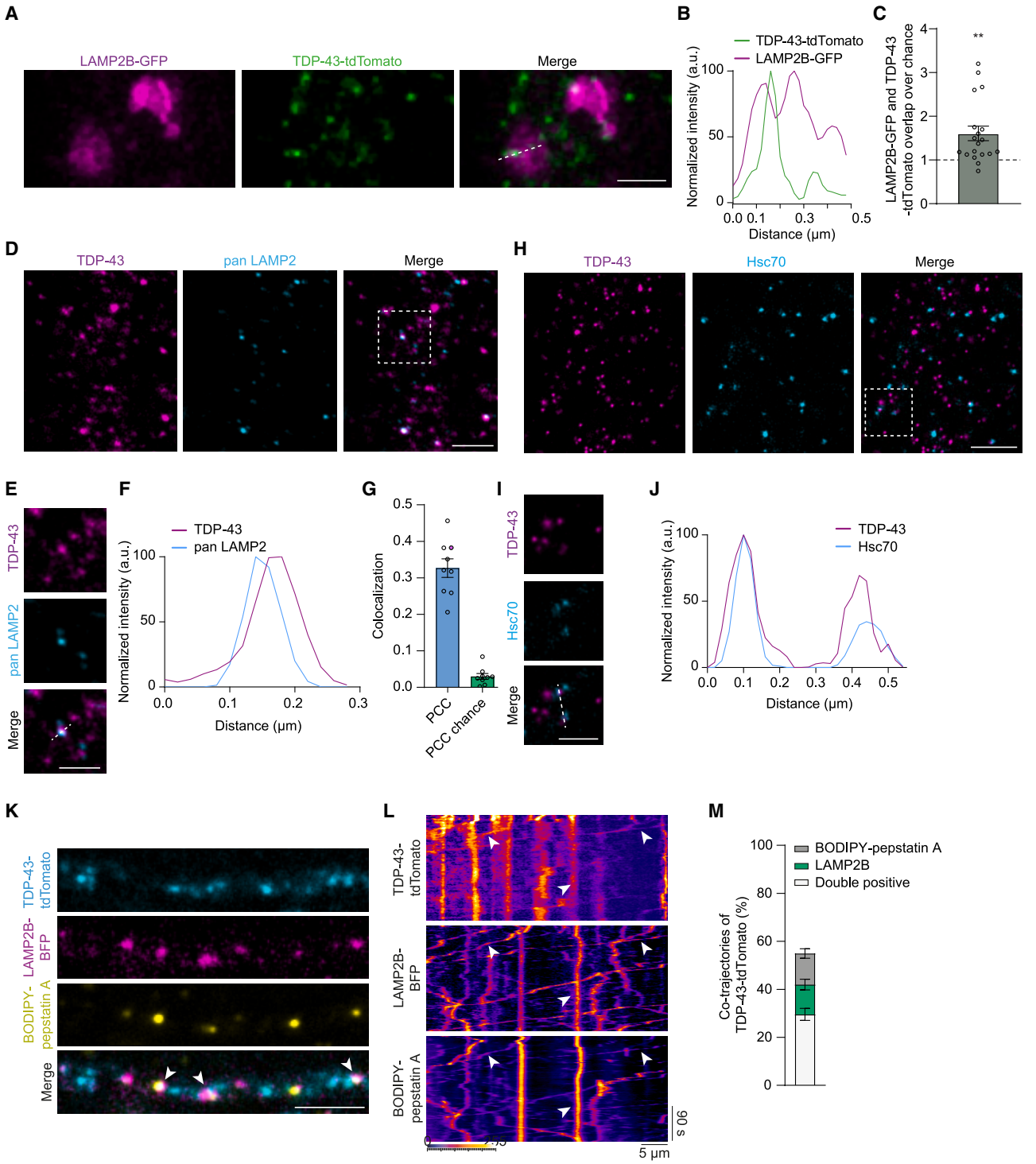

Figure 6. LAMP2B-positive lysosomes are CMA competent and associate with the CMA client TDP-43

(A) STED microscopy images showing a dendritic segment of neurons transfected with TDP-43-tdTomato and LAMP2B-GFP. Scale bar, 500 nm.

(B) Line profiles indicating the intensity of the signal, revealing an overlap of signal between TDP-43-tdTomato and LAMP2B-GFP.

(C) LAMP2B-GFP is positive for TDP-43-tdTomato significantly higher than expected due to chance (overlap with TDP-43-tdTomato channel rotated by 180°). Dashed line indicates overlap expected due to chance. n = 18 cells from 2 independent cell cultures. **p < 0.01 by one-sample t test.

(D and E) STED images of dendritic segments immunostained with TDP-43- and pan LAMP2-detecting antibodies. The dashed square indicates a ROI shown in (E). Scale bar, 500 nm.

(legend continued on next page)

in the medium at baseline are already high since cultures were kept for over 2 weeks in this medium. TDP-43 is an aggregation-prone protein and its neuronal aggregation is associated with amyotrophic lateral sclerosis (ALS) and frontotemporal dementia (FTD).[50,51] We therefore then used this assay to test whether also other dendritic proteins implied in neurodegenerative diseases are released to the extracellular space upon activation of NMDAR. To this end we chose huntingtin (Htt) and we indeed found that Htt exhibited activity-dependent release from neurons stimulated with NMDA similar to TDP-43 (Figures 7B and 7E). Interestingly, this release was not evident for α-synuclein, a causative agent involved in Parkinson's disease that is mainly present in axons (Figures 7B and 7F), indicating that NMDAR-dependent lysosomal exocytosis of CMA clients occurs primarily in dendrites.

In the final set of experiments, we bath applied the dominant-negative TAT peptide, which disrupts binding of LAMP2B to SAP102/Dlg3 and then stimulated neurons with NMDA (Figures 7G–7J). We found that the TAT peptide blocked the accumulation of TDP43, Htt, and GAPDH in the medium, a finding in support of the proposed mechanism of lysosomal stalling and exocytosis (Figures 7G–7J). Interestingly, the acute pre-treatment of cultures with 17-dimethylaminoethylamino-17-demethoxygeldanamycin, which decreases levels of lysosomal chaperons thereby acting as a CMA inhibitor,[22] abolished recruitment of tRFP-KFERQ to LAMP2B-GFP- and LAMP2A-positive membranes (Figures S7A and S7B). However, although the acute CMA impairment did not impair lysosomal exocytosis (Figures S7C–S7F), it significantly decreased the release of Htt and TDP-43 to the extracellular space upon NMDA treatment (Figures S7G–S7I).

DISCUSSION

A large number of studies have addressed local degradation by the ubiquitin proteasome system in dendrites[52]; however, much less is known about a local degradative role of lysosomes.[53,54] Here, we identify a sub-population of LAMP2A/B-positive lysosomes in dendrites that are capable to locally secrete CMA clients. We found that a direct association of LAMP2B, but not LAMP2A, with the SH3-GK domain of SAP102/Dlg3 docks exocytotic lysosomes to GluN2B-containing NMDAR, whereas LAMP2A serves as CMA receptor that enables loading of CMA clients. Upon NMDAR activation, this subpopulation of lysosomes fuse with the plasma membrane and release CMA clients to the extracellular space (Figure 7K). CMA has not been described in dendrites yet and the unexpected link between lysosome exocytosis and CMA indicates that local dendritic catabolic processes are regulated by neuronal activity and potentially serve a second function in structural plasticity that might be an inevitable consequence of the necessity for local protein disposal. Several interesting questions arise from these findings that we would like to discuss in more detail.

LAMP1 and LAMP2 label different populations of dendritic lysosomes that might serve different functions

In most previous studies the characterization of lysosomes in dendrites was based on the identification of LAMP1 or LAMP2, both of which have been frequently used interchangeably as lysosomal markers.[53,54] We observed that, in the majority of cases, LAMP1 and LAMP2 do not reside in the same vesicular membranes and that they label vesicles of distinct motility that are differentially regulated by NMDAR activation. While NMDA stimulation induced stalling of LAMP2B-positive vesicles, we could not see any change in motility of LAMP1 vesicles. Furthermore, we did not observe an activity-dependent plasma membrane fusion of SEP-tagged LAMP1. Collectively, these results indicate that dendritic subpopulations of lysosomes exist that likely have different functions.

Interestingly, both populations appear to be to a large extent catabolically active. While LAMP1 might be present on some exocytic lysosomes, the data suggest that the presence of LAMP2A/B is a prerequisite for lysosomal fusion to the plasma membrane and that the LAMP2-positive lysosome pool appears to have acquired a specific role for the disposal of CMA clients.

Lysosomes are heterogeneous single-membrane organelles defined by a highly acidic lumen (pH < 5), the presence of hydrolases, and a lack of mannose-6-phosphate receptors.[3,6] Interestingly, these criteria are not fulfilled by the majority of LAMP1-positive axonal vesicles, which are rather mildly acidic transport carriers (TCs) or early and late endosomes devoid of degradative capabilities rather than fully acidified mature lysosomes.[6,13,55] It is highly probable that, likewise, LAMP1-positive TCs constitute a portion of dendritic vesicles labeled by this marker.

The ability to degrade CMA clients may further contribute to the functional heterogeneity of LAMP1- and LAMP2-positive organelles in neurons, especially since it was previously shown that not all lysosomes are CMA competent.[14,22,56] While LAMP2A is the rate-limiting factor for the uptake of CMA clients, the CMA-competent lysosomes require also the presence of intraluminal chaperones.[14,22,57] Currently it is unclear how the presence of chaperones might contribute to lysosomal heterogeneity in dendrites.

(F) The line profiles indicate relative intensities for deconvolved STED channels.
(G) Pearson's correlation coefficient (colocalization, PCC) for endogenous LAMP2 and TDP-43. The magenta colored data point indicates the calculated PCC from the representative image. n = 9 cells from 2 independent cultures.
(H–J) Deconvolved STED images of hippocampal neurons stained against endogenous TDP-43 and Hsc70. Scale bar, 500 nm. The dashed square indicates (I) ROI and the line from which (J) line profile was generated. Scale bar, 500 nm.
(K–M) TDP-43-tdTomato co-traffics with LAMP2B-positive lysosomes. (K) TIRFM images of first frame from live-cell imaging experiments with hippocampal neurons transfected with TDP-43-tdTomato and LAMP2B-BFP incubated with BODIPY-pepstatin A . White arrows indicate colocalization. Scale bar, 5 μm. (L) Representative kymographs generated from dendritic segments of hippocampal neurons transfected with TDP-43-tdTomato and LAMP2-BFP incubated with BODIPY-pepstatin A. White arrows indicate stationary as well as mobile trajectories of LAMP2B-positive lysosomes co-trafficking with TDP-43-tdTomato.
(M) Fractions of TDP-43-tdTomato co-trafficking with LAMP2B-BFP and LAMP2B-BFP positive for BODIPY-pepstatin A. n = 24 cells from 7 independent cultures. (L) Lookup table indicates the pixel intensities from 0 to 255. (C, G and M) Data are plotted as average ±SEM.

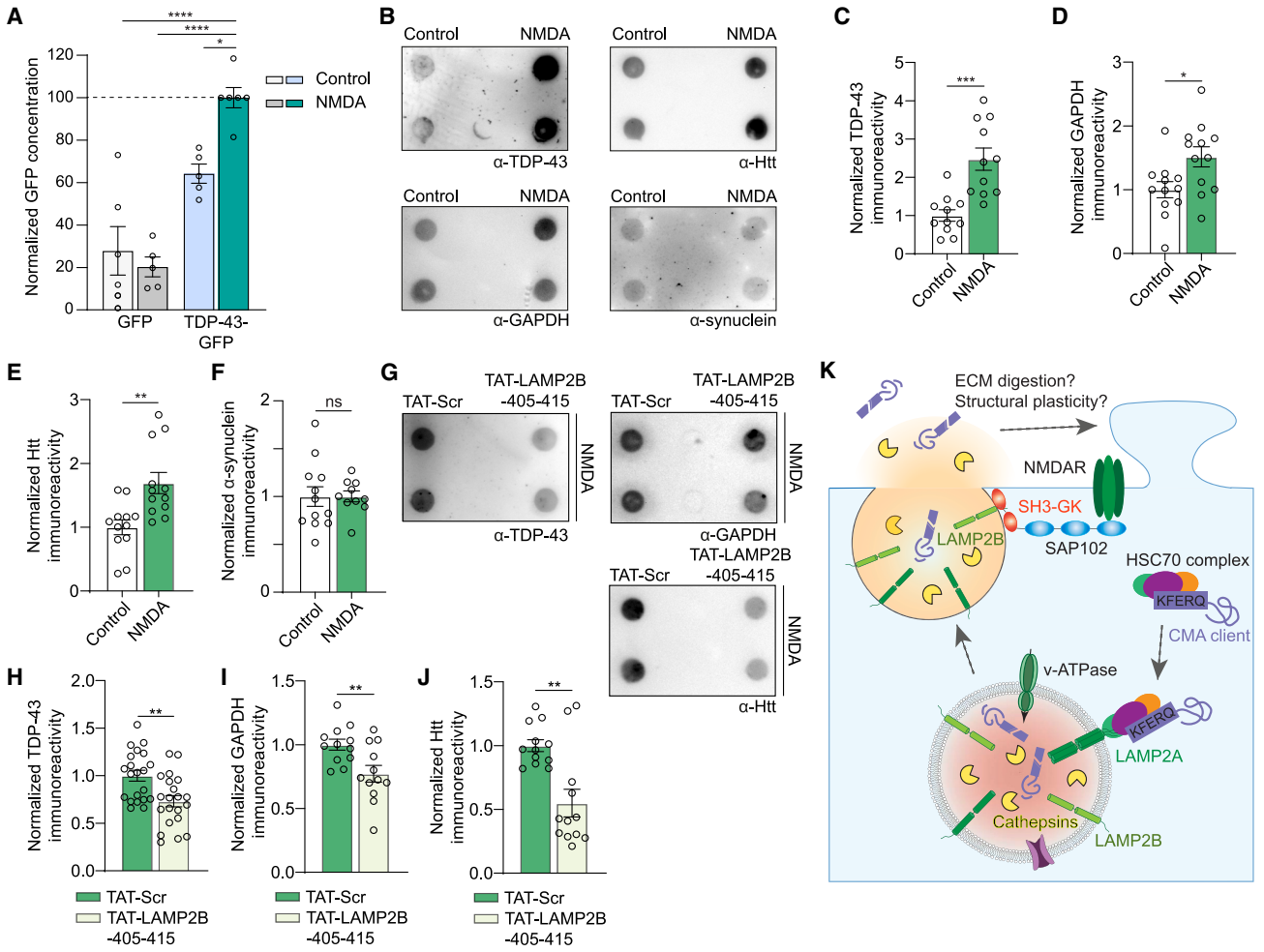

Figure 7. CMA clients are released from neurons upon stimulation with NMDA

(A) Cortical neurons were infected with AAV_GFP or AAV_TDP-43-GFP and the medium was collected after stimulation with 20 μM NMDA. The amount of GFP-tagged proteins was quantified with ELISA. n = 6 replicates from 5 independent cultures. ****$p < 0.0001$ and *$p < 0.05$ by two-way ANOVA with post hoc Tukey test.

(B) Dot blots revealed increase of extracellular TDP-43, GAPDH, Htt, and α-synuclein levels in medium collected from cortical neuronal culture (DIV16–21) after stimulation with NMDA compared with non-treated cells (control). Each dot represents independent replicates.

(C–F) Quantification of (C) TDP-43, (D) GAPDH, (E) Htt, and (F) α-synuclein dot blot immunoreactivity normalized to control. n = 11–12 replicates from at least 2 independent cultures. *$p < 0.05$, ***$p < 0.001$ by two-tailed unpaired Student's t test for TDP-43, GAPDH, and α-synuclein, **$p < 0.01$ by two-tailed Mann-Whitney U test for Htt.

(G) Dot blots revealed decreased NMDA-induced release of TDP-43, GAPDH, and Htt in neuronal cultures pre-treated with TAT-LAMP2B-405-415 peptide but not scrambled control (TAT-Scr).

(H–J) Quantification of (H) TDP-43, (I) GAPDH, and (J) Htt dot blot immunoreactivity normalized to TAT-Scr-treated NMDA-stimulated group. n = 12–21 replicates from at least 2 independent cultures. **$p < 0.01$ by two-tailed unpaired Student's t test for TDP-43, GAPDH. **$p < 0.01$ by two-tailed Mann-Whitney U test for Htt.

(K) Summary cartoon. CMA clients are targeted to the CMA-competent, LAMP2A/B-positive lysosomes. NMDA receptor activation induces direct binding of the LAMP2A/B-positive lysosomes to the SH3-GK domain of SAP102 (NMDA receptor scaffold belonging to the MAGUK family). The binding to SAP102 precedes activity-dependent fusion and release of CMA clients to the extracellular space. In addition, the release of lysosomal proteases could result in the extracellular matrix (ECM) digestion and dendritic spine remodeling. (A, C–F, and H–J) Data are plotted as average ± SEM.

LAMP2B directly binds to the GluN2B scaffold SAP102/Dlg3

The second important finding of this study concerns the stalling of LAMP2B-positive lysosomes in proximity to GluN2B-containing NMDAR, an association that is modulated by NMDAR activity (Figure 7K). This association essentially requires a direct interaction of the cytoplasmic tail of LAMP2B with the SH3-GK domain of SAP102/Dlg3, a MAGUK that will then likely interconnect lysosomes with NMDAR via an association of the PDZ domain of SAP102/Dlg3 to the PDZ-binding motif of GluN2B (Figure 7K).[37,39] What could be the reason that NMDAR activation and presumably Ca^{2+} influx regulates association with lysosomes? At present we can only speculate about a mechanism, but it is tempting to assume that folding back of the GK to the SH3 domain might be

involved. It has been so far only described for the MAGUK family member SAP97,[58,59] whereas for SAP102/Dlg3 only indirect evidence for such a mechanism has been published.[60] The intramolecular interaction results in a closed conformation and might prevent docking of lysosomes. Upon Ca^{2+} influx through NMDAR, subsequent Ca^{2+}/calmodulin binding was shown to interrupt the intramolecular interaction and could thereby render the binding interface accessible for docking of lysosomes.

Another intriguing question concerns the localization of GluN2B-SAP102/Dlg3-dependent lysosomal fusion sites. Both, GluN2B and SAP102/Dlg3 localize to synaptic and extrasynaptic sites.[61,62] It was previously demonstrated that excitatory spine synapses are transiently positive for lysosomes.[9] Our data, however, indicate that lysosomal stalling and fusion also occur in the dendritic shaft, possibly at excitatory shaft synapses[63,64] as well as extrasynaptic sites. The stimulation protocols used in the present study as well as in previous work (i.e., NMDA bath application, field stimulation, K^+-driven depolarization, back-propagating action potential)[10] directly or indirectly induce glutamate spill over resulting in activation of extrasynaptic NMDAR.[65,66]

Secretory lysosomes are linked to CMA, and lysosomal fusion leads to the release of CMA clients

Of particular interest in this scenario was the observation that LAMP2-positive lysosomes release CMA clients such as TDP-43 and Htt to the extracellular space (Figure 7). Such proteins are translocated through multimerized LAMP2A, which is the receptor and rate-limiting factor for CMA, whose upregulation significantly increases CMA rate.[17,20,22,47] CMA clients include numerous aggregation-prone proteins contributing to the onset and progression of neurodegenerative disorders, such as Htt in Huntington's disease, as well as TDP-43 in FTD and ALS.[14,15,17] Our data indicate that the release of these proteins requires both LAMP2A (CMA receptor) and LAMP2B, which enables docking to SAP102/Dlg3. This mechanism may serve to locally dispose aggregation-prone proteins and protect against proteostatic stress in neurons, which are highly polarized cells with a complex dendritic tree and thin processes. Many of these proteins belong to the so-called metastable subproteome, which is characterized by high protein concentrations relative to the solubility limit, and their supersaturation is linked to increased aggregation during stress and aging.[67] Since protein supersaturation is a function of volume,[67] it is plausible that LAMP2A/B-positive exocytic lysosomes contribute to the regulation of this metastable proteome during enhanced dendritic activity. Along these lines, the minute volume of such processes makes them vulnerable to cytoplasmic protein aggregates and lysosomal release of CMA clients could be an effective means to prevent aggregation that will likely interfere with synaptic function. Several lines of indirect evidence suggest that disruption of lysosomal function is indeed intimately linked to impairment of synaptic function in disease states associated with CMA clients such as TDP-43 and Htt.[14,15,17] Moreover, exocytosis of these proteins might also explain why they can be prominently detected in cerebrospinal fluid and the correlation of increased protein levels correlating with disease progression might be due to enhanced secretion from affected neurons subsequently cleared by the glymphatic system.

Moreover, if one assumes that a major function of LAMP2A and -2B-bearing lysosomes is dendritic release of CMA clients, an interesting question concerns how their formation is regulated. Since the presence of both LAMPs on the same vesicle is necessary for lysosomal secretion, only a subset of dendritic lysosomes is release competent. An intriguing possibility is that their biogenesis might occur on demand and that cellular stress is linked to upregulation of protein levels and increased fusion of LAMP2A and -2B-bearing vesicles.

The necessity for local disposal of CMA clients might result in local structural re-modeling of the ECM

Finally, we found that motility of LAMP2B-positive lysosomes is modulated by NMDAR activity, which induces their stalling and fusion. We could confirm previous results showing an enlargement of spine synapses in close proximity to the release site (Figure S5).[10] Taken together, both studies suggest that active cathepsins will enter the interstitial space and that cleavage of ECM components by cathepsins or matrix metalloproteases will allow for local re-modelling of the matrix and that this might in turn facilitate spine growth. It is tempting to speculate that ECM cleavage by released lysosomal proteases may also enhance lateral diffusion of receptors. This may be of particular importance, especially in case of key receptors for synaptic plasticity such as AMPAR or NMDAR.[68–70] Lysosomal fusion and subsequent ECM cleavage could mobilize the extrasynaptic AMPAR and NMDAR pool for lateral movement to synaptic sites.[68–70] What is currently lacking, however, is direct evidence that local lysosomal exocytosis is essential for synaptic function or is indeed involved in synaptic plasticity. A final intriguing question is to what extent CMA clients in exocytotic lysosomes will be degraded. These lysosomes are catabolically active but the results of the ELISA and dot blot experiments suggest that the degradation is not complete.

In summary, we propose that fusion of dendritic LAMP2A/B-positive lysosomes serves both protein removal and modulation of synaptic processes. The latter might be an inevitable consequence of the necessity for local disposal of CMA clients in dendrites. Thus, we hypothesize that the co-release of cathepsins and subsequent local proteolysis of the ECM is driven by the needs of local proteostasis.

Limitations of the study

The present study identified mature lysosomes by the use of dyes that label active lysosomal proteases. It is important to note, however, that while cathepsins display the highest activity at acidic pH some remain partially active in a broader pH range. Therefore, based on these readouts that do not determine the actual pH in the vesicles, it is not possible to exclude further heterogeneity in the population of active lysosomes.

STAR★METHODS

Detailed methods are provided in the online version of this paper and include the following:

- KEY RESOURCES TABLE
- RESOURCE AVAILABILITY

SUPPLEMENTAL INFORMATION

Supplemental information can be found online at https://doi.org/10.1016/j.celrep.2023.112998.

ACKNOWLEDGMENTS

The authors are grateful to Dr. E.D. Gundelfinger for critical comments on the manuscript. We gratefully acknowledge the professional technical assistance of M. Marunde, C. Borutzki, I. Herbert, I. Ohmert, and J. Schröder. We would like to thank Dr. J. Bär for preparation of rat hippocampal cultures, as well as Dr. C.C. Garner and Dr. U. Thomas for SAP102 constructs. We would like to thank Dr. Z. Padamsey and Dr. N. Emptage for providing SEP-LAMP2B construct. We would like to thank Dr. I. Braren from UKE vector facility and Dr. J.C. Johnston, University of Pennsylvania, USA, for AAV9 virus production.

This work was supported by grants from the Deutsche Forschungsgemeinschaft (Kr1879/10-1, CRC1436 TPA02 and TPA04, FOR2419 TP3, and FOR5228 RP6) and HFSPRGP0002/20226 (to M.R.K.), SFB841 (to D.G. and B.F.), and DFG Research Infrastructure, RI_00489 (to A.V.F.).

AUTHOR CONTRIBUTIONS

K.M.G. and M.R.K. designed the study and wrote the first draft of the paper. K.M.G., M.S., R.R., and L.L. performed the experiments. K.M.G., M.S., A.V.F., and C.S. analyzed the data. D.G. and B.F. designed the CRISPR-Cas9 gene downregulation strategy. All authors read and commented on the manuscript.

DECLARATION OF INTERESTS

The authors declare no competing interests.

Received: February 18, 2023
Revised: June 16, 2023
Accepted: August 1, 2023
Published: August 16, 2023

REFERENCES

1. Dieterich, D.C., and Kreutz, M.R. (2016). Proteomics of the Synapse–A Quantitative Approach to Neuronal Plasticity. Mol. Cell. Proteomics *15*, 368–381. https://doi.org/10.1074/mcp.R115.051482.
2. Grochowska, K.M., Andres-Alonso, M., Karpova, A., and Kreutz, M.R. (2022). The needs of a synapse-How local organelles serve synaptic proteostasis. EMBO J. *41*, e110057. https://doi.org/10.15252/embj.2021110057.
3. Saftig, P., and Klumperman, J. (2009). Lysosome biogenesis and lysosomal membrane proteins: trafficking meets function. Nat. Rev. Mol. Cell Biol. *10*, 623–635. https://doi.org/10.1038/nrm2745.
4. Luzio, J.P., Hackmann, Y., Dieckmann, N.M.G., and Griffiths, G.M. (2014). The biogenesis of lysosomes and lysosome-related organelles. Cold Spring Harbor Perspect. Biol. *6*, a016840. https://doi.org/10.1101/cshperspect.a016840.
5. Lawrence, R.E., and Zoncu, R. (2019). The lysosome as a cellular centre for signalling, metabolism and quality control. Nat. Cell Biol. *21*, 133–142. https://doi.org/10.1038/s41556-018-0244-7.
6. Lie, P.P.Y., and Nixon, R.A. (2019). Lysosome trafficking and signaling in health and neurodegenerative diseases. Neurobiol. Dis. *122*, 94–105. https://doi.org/10.1016/j.nbd.2018.05.015.
7. Yap, C.C., Digilio, L., McMahon, L.P., Garcia, A.D.R., and Winckler, B. (2018). Degradation of dendritic cargos requires Rab7-dependent transport to somatic lysosomes. J. Cell Biol. *217*, 3141–3159. https://doi.org/10.1083/jcb.201711039.
8. Cheng, X.T., Xie, Y.X., Zhou, B., Huang, N., Farfel-Becker, T., and Sheng, Z.H. (2018). Characterization of LAMP1-labeled nondegradative lysosomal and endocytic compartments in neurons. J. Cell Biol. *217*, 3127–3139. https://doi.org/10.1083/jcb.201711083.
9. Goo, M.S., Sancho, L., Slepak, N., Boassa, D., Deerinck, T.J., Ellisman, M.H., Bloodgood, B.L., and Patrick, G.N. (2017). Activity-dependent trafficking of lysosomes in dendrites and dendritic spines. J. Cell Biol. *216*, 2499–2513. https://doi.org/10.1083/jcb.201704068.
10. Padamsey, Z., McGuinness, L., Bardo, S.J., Reinhart, M., Tong, R., Hedegaard, A., Hart, M.L., and Emptage, N.J. (2017). Activity-Dependent Exocytosis of Lysosomes Regulates the Structural Plasticity of Dendritic Spines. Neuron *93*, 132–146. https://doi.org/10.1016/j.neuron.2016.11.013.
11. Sun, J., Liu, Y., Hao, X., Lin, W., Su, W., Chiang, E., Baudry, M., and Bi, X. (2022). LAMTOR1 inhibition of TRPML1-dependent lysosomal calcium release regulates dendritic lysosome trafficking and hippocampal neuronal function. EMBO J. *41*, e108119. https://doi.org/10.15252/embj.2021108119.
12. Vukoja, A., Rey, U., Petzoldt, A.G., Ott, C., Vollweiter, D., Quentin, C., Puchkov, D., Reynolds, E., Lehmann, M., Hohensee, S., et al. (2018). Presynaptic Biogenesis Requires Axonal Transport of Lysosome-Related Vesicles. Neuron *99*, 1216–1232.e7. https://doi.org/10.1016/j.neuron.2018.08.004.
13. Lie, P.P.Y., Yang, D.S., Stavrides, P., Goulbourne, C.N., Zheng, P., Mohan, P.S., Cataldo, A.M., and Nixon, R.A. (2021). Post-Golgi carriers, not lysosomes, confer lysosomal properties to pre-degradative organelles in normal and dystrophic axons. Cell Rep. *35*, 109034. https://doi.org/10.1016/j.celrep.2021.109034.
14. Kaushik, S., and Cuervo, A.M. (2018). The coming of age of chaperone-mediated autophagy. Nat. Rev. Mol. Cell Biol. *19*, 365–381. https://doi.org/10.1038/s41580-018-0001-6.
15. Alfaro, I.E., Albornoz, A., Molina, A., Moreno, J., Cordero, K., Criollo, A., and Budini, M. (2018). Chaperone Mediated Autophagy in the Crosstalk

of Neurodegenerative Diseases and Metabolic Disorders. Front. Endocrinol. *9*, 778. https://doi.org/10.3389/fendo.2018.00778.

16. Fleming, A., Bourdenx, M., Fujimaki, M., Karabiyik, C., Krause, G.J., Lopez, A., Martín-Segura, A., Puri, C., Scrivo, A., Skidmore, J., et al. (2022). The different autophagy degradation pathways and neurodegeneration. Neuron *110*, 935–966. https://doi.org/10.1016/j.neuron.2022.01.017.
17. Bourdenx, M., Gavathiotis, E., and Cuervo, A.M. (2021). Chaperone-mediated autophagy: a gatekeeper of neuronal proteostasis. Autophagy *17*, 2040–2042. https://doi.org/10.1080/15548627.2021.1935007.
18. Kirchner, P., Bourdenx, M., Madrigal-Matute, J., Tiano, S., Diaz, A., Bartholdy, B.A., Will, B., and Cuervo, A.M. (2022). Correction: Proteome-wide analysis of chaperone-mediated autophagy targeting motifs. PLoS Biol. *20*, e3001550. https://doi.org/10.1371/journal.pbio.3001550.
19. Dong, S., Aguirre-Hernandez, C., Scrivo, A., Eliscovich, C., Arias, E., Bravo-Cordero, J.J., and Cuervo, A.M. (2020). Monitoring spatiotemporal changes in chaperone-mediated autophagy in vivo. Nat. Commun. *11*, 645. https://doi.org/10.1038/s41467-019-14164-4.
20. Patel, B., and Cuervo, A.M. (2015). Methods to study chaperone-mediated autophagy. Methods *75*, 133–140. https://doi.org/10.1016/j.ymeth.2015.01.003.
21. Cuervo, A.M. (2010). Chaperone-mediated autophagy: selectivity pays off. Trends Endocrinol. Metabol. *21*, 142–150. https://doi.org/10.1016/j.tem.2009.10.003.
22. Bandyopadhyay, U., Kaushik, S., Varticovski, L., and Cuervo, A.M. (2008). The chaperone-mediated autophagy receptor organizes in dynamic protein complexes at the lysosomal membrane. Mol. Cell Biol. *28*, 5747–5763. https://doi.org/10.1128/mcb.02070-07.
23. Wang, Y., Martinez-Vicente, M., Krüger, U., Kaushik, S., Wong, E., Mandelkow, E.M., Cuervo, A.M., and Mandelkow, E. (2009). Tau fragmentation, aggregation and clearance: the dual role of lysosomal processing. Hum. Mol. Genet. *18*, 4153–4170. https://doi.org/10.1093/hmg/ddp367.
24. Cuervo, A.M., Stefanis, L., Fredenburg, R., Lansbury, P.T., and Sulzer, D. (2004). Impaired Degradation of Mutant α-Synuclein by Chaperone-Mediated Autophagy. Science *305*, 1292–1295. https://doi.org/10.1126/science.1101738.
25. Eskelinen, E.-L., Cuervo, A.M., Taylor, M.R.G., Nishino, I., Blum, J.S., Dice, J.F., Sandoval, I.V., Lippincott-Schwartz, J., August, J.T., and Saftig, P. (2005). Unifying Nomenclature for the Isoforms of the Lysosomal Membrane Protein LAMP-2. Traffic *6*, 1058–1061. https://doi.org/10.1111/j.1600-0854.2005.00337.x.
26. Endo, Y., Furuta, A., and Nishino, I. (2015). Danon disease: a phenotypic expression of LAMP-2 deficiency. Acta Neuropathol. *129*, 391–398. https://doi.org/10.1007/s00401-015-1385-4.
27. Rothaug, M., Stroobants, S., Schweizer, M., Peters, J., Zunke, F., Allerding, M., D'Hooge, R., Saftig, P., and Blanz, J. (2015). LAMP-2 deficiency leads to hippocampal dysfunction but normal clearance of neuronal substrates of chaperone-mediated autophagy in a mouse model for Danon disease. Acta Neuropathol. Commun. *3*, 6. https://doi.org/10.1186/s40478-014-0182-y.
28. Chen, C.S., Chen, W.N., Zhou, M., Arttamangkul, S., and Haugland, R.P. (2000). Probing the cathepsin D using a BODIPY FL-pepstatin A: applications in fluorescence polarization and microscopy. J. Biochem. Biophys. Methods *42*, 137–151. https://doi.org/10.1016/s0165-022x(00)00048-8.
29. Paoletti, P., Bellone, C., and Zhou, Q. (2013). NMDA receptor subunit diversity: impact on receptor properties, synaptic plasticity and disease. Nat. Rev. Neurosci. *14*, 383–400. https://doi.org/10.1038/nrn3504.
30. Hardingham, G.E., and Bading, H. (2010). Synaptic versus extrasynaptic NMDA receptor signalling: implications for neurodegenerative disorders. Nat. Rev. Neurosci. *11*, 682–696. https://doi.org/10.1038/nrn2911.
31. Kopec, C.D., Li, B., Wei, W., Boehm, J., and Malinow, R. (2006). Glutamate receptor exocytosis and spine enlargement during chemically induced long-term potentiation. J. Neurosci. *26*, 2000–2009. https://doi.org/10.1523/jneurosci.3918-05.2006.
32. Hämälistö, S., Stahl, J.L., Favaro, E., Yang, Q., Liu, B., Christoffersen, L., Loos, B., Guasch Boldú, C., Joyce, J.A., Reinheckel, T., et al. (2020). Spatially and temporally defined lysosomal leakage facilitates mitotic chromosome segregation. Nat. Commun. *11*, 229. https://doi.org/10.1038/s41467-019-14009-0.
33. Shen, Y., Rosendale, M., Campbell, R.E., and Perrais, D. (2014). pHuji, a pH-sensitive red fluorescent protein for imaging of exo- and endocytosis. J. Cell Biol. *207*, 419–432. https://doi.org/10.1083/jcb.201404107.
34. Dinamarca, M.C., Guzzetti, F., Karpova, A., Lim, D., Mitro, N., Musardo, S., Mellone, M., Marcello, E., Stanic, J., Samaddar, T., et al. (2016). Ring finger protein 10 is a novel synaptonuclear messenger encoding activation of NMDA receptors in hippocampus. Elife *5*, e12430. https://doi.org/10.7554/eLife.12430.
35. Melgarejo da Rosa, M., Yuanxiang, P., Brambilla, R., Kreutz, M.R., and Karpova, A. (2016). Synaptic GluN2B/CaMKII-α Signaling Induces Synapto-Nuclear Transport of ERK and Jacob. Front. Mol. Neurosci. *9*, 66. https://doi.org/10.3389/fnmol.2016.00066.
36. Delgado, J.Y., Fink, A.E., Grant, S.G.N., O'Dell, T.J., and Opazo, P. (2018). Rapid homeostatic downregulation of LTP by extrasynaptic GluN2B receptors. J. Neurophysiol. *120*, 2351–2357. https://doi.org/10.1152/jn.00421.2018.
37. Chen, B.S., Gray, J.A., Sanz-Clemente, A., Wei, Z., Thomas, E.V., Nicoll, R.A., and Roche, K.W. (2012). SAP102 mediates synaptic clearance of NMDA receptors. Cell Rep. *2*, 1120–1128. https://doi.org/10.1016/j.celrep.2012.09.024.
38. Wei, Z., Behrman, B., Wu, W.H., and Chen, B.S. (2015). Subunit-specific regulation of N-methyl-D-aspartate (NMDA) receptor trafficking by SAP102 protein splice variants. J. Biol. Chem. *290*, 5105–5116. https://doi.org/10.1074/jbc.M114.599969.
39. Vieira, M., Yong, X.L.H., Roche, K.W., and Anggono, V. (2020). Regulation of NMDA glutamate receptor functions by the GluN2 subunits. J. Neurochem. *154*, 121–143. https://doi.org/10.1111/jnc.14970.
40. Elias, G.M., and Nicoll, R.A. (2007). Synaptic trafficking of glutamate receptors by MAGUK scaffolding proteins. Trends Cell Biol. *17*, 343–352. https://doi.org/10.1016/j.tcb.2007.07.005.
41. Seitz, K.J., and Rizzoli, S.O. (2019). GFP nanobodies reveal recently-exocytosed pHluorin molecules. Sci. Rep. *9*, 7773. https://doi.org/10.1038/s41598-019-44262-8.
42. Bera, S., Raghuram, V., Mikhaylova, M., and Kreutz, M.R. (2016). A plasmid-based expression system to study protein-protein interactions at the Golgi in vivo. Anal. Biochem. *502*, 50–52. https://doi.org/10.1016/j.ab.2016.02.016.
43. Lukinavičius, G., Reymond, L., Umezawa, K., Sallin, O., D'Este, E., Göttfert, F., Ta, H., Hell, S.W., Urano, Y., and Johnsson, K. (2016). Fluorogenic Probes for Multicolor Imaging in Living Cells. J. Am. Chem. Soc. *138*, 9365–9368. https://doi.org/10.1021/jacs.6b04782.
44. Rout, A.K., Strub, M.P., Piszczek, G., and Tjandra, N. (2014). Structure of transmembrane domain of lysosome-associated membrane protein type 2a (LAMP-2A) reveals key features for substrate specificity in chaperone-mediated autophagy. J. Biol. Chem. *289*, 35111–35123. https://doi.org/10.1074/jbc.M114.609446.
45. Cuervo, A.M., and Dice, J.F. (2000). Unique properties of lamp2a compared to other lamp2 isoforms. J. Cell Sci. *113 Pt 24*, 4441–4450. https://doi.org/10.1242/jcs.113.24.4441.
46. Koga, H., Martinez-Vicente, M., Macian, F., Verkhusha, V.V., and Cuervo, A.M. (2011). A photoconvertible fluorescent reporter to track chaperone-mediated autophagy. Nat. Commun. *2*, 386. https://doi.org/10.1038/ncomms1393.
47. Anguiano, J., Garner, T.P., Mahalingam, M., Das, B.C., Gavathiotis, E., and Cuervo, A.M. (2013). Chemical modulation of chaperone-mediated autophagy by retinoic acid derivatives. Nat. Chem. Biol. *9*, 374–382. https://doi.org/10.1038/nchembio.1230.

48. Ormeño, F., Hormazabal, J., Moreno, J., Riquelme, F., Rios, J., Criollo, A., Albornoz, A., Alfaro, I.E., and Budini, M. (2020). Chaperone Mediated Autophagy Degrades TDP-43 Protein and Is Affected by TDP-43 Aggregation. Front. Mol. Neurosci. *13*, 19. https://doi.org/10.3389/fnmol.2020.00019.

49. Yang, C., Tan, W., Whittle, C., Qiu, L., Cao, L., Akbarian, S., and Xu, Z. (2010). The C-terminal TDP-43 fragments have a high aggregation propensity and harm neurons by a dominant-negative mechanism. PLoS One *5*, e15878. https://doi.org/10.1371/journal.pone.0015878.

50. Ling, S.C., Polymenidou, M., and Cleveland, D.W. (2013). Converging mechanisms in ALS and FTD: disrupted RNA and protein homeostasis. Neuron *79*, 416–438. https://doi.org/10.1016/j.neuron.2013.07.033.

51. Mackenzie, I.R., Rademakers, R., and Neumann, M. (2010). TDP-43 and FUS in amyotrophic lateral sclerosis and frontotemporal dementia. Lancet Neurol. *9*, 995–1007. https://doi.org/10.1016/s1474-4422(10)70195-2.

52. Tai, H.C., and Schuman, E.M. (2008). Ubiquitin, the proteasome and protein degradation in neuronal function and dysfunction. Nat. Rev. Neurosci. *9*, 826–838. https://doi.org/10.1038/nrn2499.

53. Yap, C.C., Mason, A.J., and Winckler, B. (2022). Dynamics and distribution of endosomes and lysosomes in dendrites. Curr. Opin. Neurobiol. *74*, 102537. https://doi.org/10.1016/j.conb.2022.102537.

54. Kononenko, N.L. (2017). Lysosomes convene to keep the synapse clean. J. Cell Biol. *216*, 2251–2253. https://doi.org/10.1083/jcb.201707070.

55. Lie, P.P.Y., Yoo, L., Goulbourne, C.N., Berg, M.J., Stavrides, P., Huo, C., Lee, J.-H., and Nixon, R.A. (2022). Axonal transport of late endosomes and amphisomes is selectively modulated by local Ca^{2+} efflux and disrupted by PSEN1 loss of function. Sci. Adv. *8*, eabj5716. https://doi.org/10.1126/sciadv.abj5716.

56. Cuervo, A.M., Dice, J.F., and Knecht, E. (1997). A population of rat liver lysosomes responsible for the selective uptake and degradation of cytosolic proteins. J. Biol. Chem. *272*, 5606–5615. https://doi.org/10.1074/jbc.272.9.5606.

57. Orenstein, S.J., and Cuervo, A.M. (2010). Chaperone-mediated autophagy: molecular mechanisms and physiological relevance. Semin. Cell Dev. Biol. *21*, 719–726. https://doi.org/10.1016/j.semcdb.2010.02.005.

58. Paarmann, I., Spangenberg, O., Lavie, A., and Konrad, M. (2002). Formation of Complexes between Ca^{2+} Calmodulin and the Synapse-associated Protein SAP97 Requires the SH3 Domain-Guanylate Kinase Domain-connecting HOOK Region. J. Biol. Chem. *277*, 40832–40838. https://doi.org/10.1074/jbc.m205618200.

59. Wu, H., Reissner, C., Kuhlendahl, S., Coblentz, B., Reuver, S., Kindler, S., Gundelfinger, E.D., and Garner, C.C. (2000). Intramolecular interactions regulate SAP97 binding to GKAP. EMBO J. *19*, 5740–5751. https://doi.org/10.1093/emboj/19.21.5740.

60. Masuko, N., Makino, K., Kuwahara, H., Fukunaga, K., Sudo, T., Araki, N., Yamamoto, H., Yamada, Y., Miyamoto, E., and Saya, H. (1999). Interaction of NE-dlg/SAP102, a Neuronal and Endocrine Tissue-specific Membrane-associated Guanylate Kinase Protein, with Calmodulin and PSD-95/SAP90. J. Biol. Chem. *274*, 5782–5790. https://doi.org/10.1074/jbc.274.9.5782.

61. Bading, H. (2017). Therapeutic targeting of the pathological triad of extrasynaptic NMDA receptor signaling in neurodegenerations. J. Exp. Med. *214*, 569–578. https://doi.org/10.1084/jem.20161673.

62. Parsons, M.P., and Raymond, L.A. (2014). Extrasynaptic NMDA receptor involvement in central nervous system disorders. Neuron *82*, 279–293. https://doi.org/10.1016/j.neuron.2014.03.030.

63. van Bommel, B., Konietzny, A., Kobler, O., Bär, J., and Mikhaylova, M. (2019). F-actin patches associated with glutamatergic synapses control positioning of dendritic lysosomes. EMBO J. *38*, e101183. https://doi.org/10.15252/embj.2018101183.

64. Bourne, J.N., and Harris, K.M. (2011). Coordination of size and number of excitatory and inhibitory synapses results in a balanced structural plasticity along mature hippocampal CA1 dendrites during LTP. Hippocampus *21*, 354–373. https://doi.org/10.1002/hipo.20768.

65. Kullmann, D.M., and Asztely, F. (1998). Extrasynaptic glutamate spillover in the hippocampus: evidence and implications. Trends Neurosci. *21*, 8–14. https://doi.org/10.1016/s0166-2236(97)01150-8.

66. Harris, A.Z., and Pettit, D.L. (2008). Recruiting extrasynaptic NMDA receptors augments synaptic signaling. J. Neurophysiol. *99*, 524–533. https://doi.org/10.1152/jn.01169.2007.

67. Ciryam, P., Tartaglia, G.G., Morimoto, R.I., Dobson, C.M., and Vendruscolo, M. (2013). Widespread aggregation and neurodegenerative diseases are associated with supersaturated proteins. Cell Rep. *5*, 781–790. https://doi.org/10.1016/j.celrep.2013.09.043.

68. Frischknecht, R., Heine, M., Perrais, D., Seidenbecher, C.I., Choquet, D., and Gundelfinger, E.D. (2009). Brain extracellular matrix affects AMPA receptor lateral mobility and short-term synaptic plasticity. Nat. Neurosci. *12*, 897–904. https://doi.org/10.1038/nn.2338.

69. Wlodarczyk, J., Mukhina, I., Kaczmarek, L., and Dityatev, A. (2011). Extracellular matrix molecules, their receptors, and secreted proteases in synaptic plasticity. Dev. Neurobiol. *71*, 1040–1053. https://doi.org/10.1002/dneu.20958.

70. Dankovich, T.M., and Rizzoli, S.O. (2022). The Synaptic Extracellular Matrix: Long-Lived, Stable, and Still Remarkably Dynamic. Front. Synaptic Neurosci. *14*, 854956. https://doi.org/10.3389/fnsyn.2022.854956.

71. Platt, R.J., Chen, S., Zhou, Y., Yim, M.J., Swiech, L., Kempton, H.R., Dahlman, J.E., Parnas, O., Eisenhaure, T.M., Jovanovic, M., et al. (2014). CRISPR-Cas9 knockin mice for genome editing and cancer modeling. Cell *159*, 440–455. https://doi.org/10.1016/j.cell.2014.09.014.

72. Schwenk, F., Baron, U., and Rajewsky, K. (1995). A cre-transgenic mouse strain for the ubiquitous deletion of loxP-flanked gene segments including deletion in germ cells. Nucleic Acids Res. *23*, 5080–5081. https://doi.org/10.1093/nar/23.24.5080.

73. Andres-Alonso, M., Ammar, M.R., Butnaru, I., Gomes, G.M., Acuña Sanhueza, G., Raman, R., Yuanxiang, P., Borgmeyer, M., Lopez-Rojas, J., Raza, S.A., et al. (2019). SIPA1L2 controls trafficking and local signaling of TrkB-containing amphisomes at presynaptic terminals. Nat. Commun. *10*, 5448. https://doi.org/10.1038/s41467-019-13224-z.

74. Gee, C.E., Ohmert, I., Wiegert, J.S., and Oertner, T.G. (2017). Preparation of Slice Cultures from Rodent Hippocampus. Cold Spring Harb. Protoc. *2017*, pdb.prot094888. https://doi.org/10.1101/pdb.prot094888.

75. Karpova, A., Mikhaylova, M., Bera, S., Bär, J., Reddy, P.P., Behnisch, T., Rankovic, V., Spilker, C., Bethge, P., Sahin, J., et al. (2013). Encoding and transducing the synaptic or extrasynaptic origin of NMDA receptor signals to the nucleus. Cell *152*, 1119–1133. https://doi.org/10.1016/j.cell.2013.02.002.

76. Mikhaylova, M., Bär, J., van Bommel, B., Schätzle, P., YuanXiang, P., Raman, R., Hradsky, J., Konietzny, A., Loktionov, E.Y., Reddy, P.P., et al. (2018). Caldendrin Directly Couples Postsynaptic Calcium Signals to Actin Remodeling in Dendritic Spines. Neuron *97*, 1110–1125.e14. https://doi.org/10.1016/j.neuron.2018.01.046.

77. Schindelin, J., Arganda-Carreras, I., Frise, E., Kaynig, V., Longair, M., Pietzsch, T., Preibisch, S., Rueden, C., Saalfeld, S., Schmid, B., et al. (2012). Fiji: an open-source platform for biological-image analysis. Nat. Methods *9*, 676–682. https://doi.org/10.1038/nmeth.2019.

78. Wiegert, J.S., Pulin, M., Gee, C.E., and Oertner, T.G. (2018). The fate of hippocampal synapses depends on the sequence of plasticity-inducing events. Elife *7*, e39151. https://doi.org/10.7554/eLife.39151.

79. Mangeol, P., Prevo, B., and Peterman, E.J.G. (2016). KymographClear and KymographDirect: two tools for the automated quantitative analysis of molecular and cellular dynamics using kymographs. Mol. Biol. Cell *27*, 1948–1957. https://doi.org/10.1091/mbc.E15-06-0404.

STAR★METHODS

KEY RESOURCES TABLE

REAGENT or RESOURCE	SOURCE	IDENTIFIER
Antibodies		
Mouse anti-LAMP1 (LY1C6)	Thermo Fisher Scientific	Cat.: #MA1-164; RRID: AB_2536869
Rat anti-LAMP2 (GL2A7)	Thermo Fisher Scientific	Cat.: #MA1-165; RRID: AB_2609332
Mouse anti-LAMP2 (H4B4)	Santa Cruz Biotechnology	Cat.: #sc-18822; RRID: AB_626858
Rabbit anti-GluN2B	Alomone Labs	Cat.: #AGC-003; RRID: AB_2040028
Guinea pig anti-Shank3	Synaptic Systems	Cat.: #162.304; RRID: AB_2619863
Mouse anti-Bassoon (SAP7F407)	Enzo	Cat.: #ADI-VAM-PS003; RRID: AB_10618753
Guinea pig anti-SAP102	Synaptic Systems	Cat.: #124.214; RRID: AB_2619803
Rabbit anti-SAP102	Synaptic Systems	Cat.: #124.202; RRID: AB_887711
Guinea pig anti-MAP2	Synaptic Systems	Cat.: #188.004; RRID: AB_2138181
Guinea pig anti-LAMP2A	Synaptic Systems	Cat.: #437.005; RRID: AB_2814937
Mouse anti-Hsc70	Synaptic Systems	Cat.: #149.011; RRID: AB_887904
Rabbit anti-tRFP	Evrogen	Cat.: #AB233; RRID: AB_2571743
Mouse anti-GFP (B34)	BioLegend	Cat.: #902601; RRID: AB_2565021
Rabbit anti-TDP-43	Proteintech	Cat.: #10782-2-AP; RRID: AB_615042
Rabbit anti-RFP	Rockland	Cat.: #600-401-379; RRID: AB_2209751
Rabbit anti-Huntingtin (Htt)	Cell Signaling Technology	Cat.: #5656; RRID: AB_10827977
Mouse anti-GAPDH	Thermo Fisher Scientific	Cat.: #MA-15738; RRID: AB_10977387
Rabbit anti-α-synuclein (D37A6)	Cell Signaling Technology	Cat.: #4179; RRID: AB_1904156
Mouse anti-synaptotagmin1 Oyster650	Synaptic Systems	Cat.: #105 311C5; RRID: AB_2619761
Anti-mouse Alexa Fluor 568	Thermo Fisher Scientific	Cat.: #A-11004; RRID: AB_2534072
Anti-mouse Alexa Fluor 647	Thermo Fisher Scientific	Cat.: #A-21235; RRID: AB_2535804
Anti-rabbit Alexa Fluor 488	Thermo Fisher Scientific	Cat.: #A-11034; RRID: AB_2576217
Anti-rabbit Alexa Fluor 568	Thermo Fisher Scientific	Cat.: #A-11036; RRID: AB_10563566
Anti-rabbit Alexa Fluor 647	Thermo Fisher Scientific	Cat.: #A-21236; RRID: AB_2535805
Anti-guinea pig Alexa Fluor 405	Abcam	Cat.: #ab175678; RRID: AB_2827755
Anti-guinea pig Alexa Fluor 488	Thermo Fisher Scientific	Cat.: #A-11073; RRID: AB_2534117
Anti-guinea pig Alexa Fluor 568	Thermo Fisher Scientific	Cat.: #A-11075; RRID: AB_2534119
Anti-guinea pig Alexa Fluor 647	Thermo Fisher Scientific	Cat.: #A-21450; RRID: AB_2535867
Anti-mouse-Abberior STAR 635P	Abberior	Cat.: #2-0002-007-5; RRID: AB_2893232
Anti-rabbit-IgG-HRP	Dianova	Cat.: #111-035-114; RRID: AB_2337938
Anti-mouse-IgG-HRP	Dianova	Cat.: #115-035-146; RRID: AB_2307392
Anti-rat abberior STAR RED	Abberior	Cat.: #STRED-1007-500UG; RRID: AB_2910106
Anti-rabbit aberrior STAR RED	Abberior	Cat.: #STRED-1002-500UG; RRID: AB_2833015
Anti-mouse Alexa Fluor 594	antibodies online	Cat.: #ABIN2667003;
Anti-rabbit Alexa Fluor 594	antibodies online	Cat.: #ABIN266002;
Anti-guinea pig Alexa Fluor 594	antibodies online	Cat.: #ABIN5660354;
Anti-GFP FluoTag-X4	Nanotag Biotechnologies	Cat.: #N0304-Af-647-L; RRID: AB_2905517
Anti-GFP FluoTag-Q	Nanotag Biotechnologies	Cat.: #N0301-AF-647-L; RRID: AB_2905515
Bacterial and virus strains		
E.coli XL10Gold	Agilent	Cat.: #200314
+E.coli Bl21DE3	Invitrogen	Cat.: #C6000-03

(*Continued on next page*)

Continued

REAGENT or RESOURCE	SOURCE	IDENTIFIER
Chemicals, peptides, and recombinant proteins		
Lipofectamine 2000	ThermoFisher Scientific	Cat.: #11668019
MaxPEI	Polysciences	Cat.: #23966
HisPur™ Ni-NTA resin	Thermo Fisher Scientific	Cat.: #88221
protease inhibitors, Complete	Roche	Cat.: # 04693159001
phosphatase inhibitors, PhosSTOP	Roche	Cat.: #04906837001
μMACS Anti-GFP MicroBeads	Miltenyi Biotec	Cat.: #130-091-125
TAT-LAMP2B-404-415 YGRKKRRQRRRGRRKTYAGYQTL	Genosphere biotechnologies	This study
TAT-Scrambled (Scr) YGRKKRRQRRRYKTAQYRLTGRG	Genosphere biotechnologies	This study
Bafilomycin A1	Sigma Aldrich	Cat.: #196000
NMDA	Sigma Aldrich	Cat.: #M3262
SiR-Lysosome	Spirochrome	Cat.: #SC012
BODIPY FL pepstatin A	Thermo Fischer Scientific	Cat.: #P12271
Magic Red™ Cathepsin B Kit	Bio-Rad	Cat.: #ICT937
17-Dimethylaminoethylamino-17-demethoxygeldanamycin (17-DMAG)	Merck	Cat.: #D5193
CA77.1	MedChemExpress	Cat.: #HY-134923
Critical commercial assays		
GFP ELISA Kit	Abcam	Cat.: #ab171581
Experimental models: Cell lines		
Human: HEK293T cells	ATCC	Cat.: #CRL-3216
African Green Monkey SV40-transformed kidney fibroblast (COS-7)	ATCC	Cat.: #CRL-1651
Experimental models: Organisms/strains		
Rat: Wistar	Janvier	RjHan:WI
Mouse: B6; 129-Gt(ROSA) 26Sor$^{tm1(CAG-cas9*,-EGFP)Fezh}$/J	Jackson laboratory	#024857[71]
Mouse: CMV-Cre-deleter	ZMNH cohort	Schwenk et al.[72]
Oligonucleotides		
GluN2B gRNA, mouse, #1: 5′-GTTGGCCGTCTTGGCCGTAT-3′	This study, Dr. Dawid Głów	N/A
GluN2B gRNA, mouse, #2: 5′-GTGTTCGGACAGCATGTCCG-3′	This study, Dr. Dawid Głów	N/A
SAP102 gRNA, mouse, 5′- GGCCCTGTTT GATTATGAT-3′	This study, Dr. Dawid Głów	N/A
LAMP2 gRNA, mouse, 5′- GCGAGCCCGTA ACCGGAGAG-3′	This study, Dr. Dawid Głów	N/A
Recombinant DNA		
Syn-GFP in pAAV9	This paper	N/A
tRFP-KFERQ in pAAV9	This paper	N/A
Human TDP-43-GFP in pAAV	This paper	N/A
EBFP2-N1	Addgene (M. Davidson)	Cat.: #54595
TREMARCKS-GFP-H1	Mikhaylova et al.[76]	N/A
pEGFP-C3	Clontech	Cat.: #6082-1
Rat SAP102 in pEGFP-C3	This paper	N/A
Rat SAP102-PDZ1-3 in pEGFP-C3	This paper	N/A
Rat SAP102-SH3-GK in pEGFP-C3	This paper	N/A
pEGFP-N1	Clontech	Cat.: #6085-1

(*Continued on next page*)

Continued

REAGENT or RESOURCE	SOURCE	IDENTIFIER
Rat GluN2B-840–1482 in pEGFP-N1	This paper	N/A
Rat LAMP1 in pEGFP-N1	This paper	N/A
ptRFP-N1	Evrogen	Cat.: #FP142
Rat GluN2B-840–1482 in ptRFP	This paper	N/A
Mouse LAMP2B in ptRFP	This paper	N/A
Human PEX3 in ptRFP	This paper	N/A
Champion pET-6xHis-SUMO	Thermo Fisher Scientific	Cat.: #K3001
Mouse/rat LAMP2B-404–415 in pET-6xHis-SUMO	This paper	N/A
Mouse/rat LAMP2A-404–415 in pET-6xHis-SUMO	This paper	N/A
pCI-synapsin-mKate2	Prof. T. Oertner	N/A
Rat LAMP1 in pCI-synapsin-mKate2-N	This paper	N/A
Mouse LAMP2B in pCI-synapsin-mKate2-N	This paper	N/A
Mouse pCI-Syn-LAMP2B-EBFP2	This paper	N/A
Mouse pCI-Syn-LAMP2B-EGFP	This paper	N/A
mCerulean	Prof. T. Oertner[78]	N/A
pGolt-mCherry	Bera et al.[42]	N/A
Mouse pGolt-mCherry-LAMP2B-404-415	This paper	N/A
Rat pGolt-mCherry-GluN2B-840-11482	This paper	N/A
pDisplay-pHuji	Addgene, Shen et al.[33]	Cat.: #61556
Mouse pCI-Syn-pHuji-LAMP2B	This paper	N/A
Rat SEP-GluN2B	Addgene, Kopec et al.[31]	Cat.: #23998
Rat pCI-Syn-SEP-LAMP1	This paper	N/A
Mouse SEP-LAMP2B	Prof. N.J. Emptage, Padamsey et al.[10]	N/A
Mouse pCI-Syn-SEP-LAMP2B	This paper	N/A
Rat pmCherry-Jacob	This paper	N/A
Human wtTDP43tdTOMATO-HA	Addgene, Yang et al.[49]	Cat.: #28205
pRNAT-U6.1	Gene script	Discontinued
LAMP1 shRNA in p RNAT-U6.1: 5′-CCAG TGTGTCCAAGTACAA-3′	This paper	N/A
Scr shRNA in pRNAT-U6.1:5′ GGATGAGT CCTCCATGTTCT-3′	Karpova et al.[75]	N/A
Software and algorithms		
(Fiji is just) ImageJ	Schindelin et al.[77]	https://fiji.sc/RRID:SCR_002285
Prism Version 9	GaphPad	https://www.graphpad.com/scientific-software/prism/
Imspector Version 16.3.13033-w2049	Aberrior instruments	https://imspector.abberior-instruments.com/
Python Version 3.8	Python	https://www.python.org/

RESOURCE AVAILABILITY

Lead contact

Further information and requests for resources and reagents should be directed to and will be fulfilled by the lead contact, Michael R. Kreutz (michael.kreutz@zmnh.uni-hamburg.de).

Materials availability

Plasmids generated in this study will be shared by the lead contact upon request upon completion of a Material Transfer Agreement.

Data and code availability

- All data reported in this paper will be shared by the lead contact upon request.
- This paper does not report original code.
- Any additional information required to reanalyze the data reported in this paper is available from the lead contact upon request.

EXPERIMENTAL MODEL AND STUDY PARTICIPANT DETAILS

Animals

All animals were obtained from colonies established at University Medical Center Hamburg-Eppendorf. All procedures were carried out in accordance with AARIVE guidelines for animal experimentation, with approval of the ethics committees of the city-state of Hamburg (Behörde für Gesundheit und Verbraucherschutz, Fachbereich Veterinärwesen) and the animal care committee of the University Medical Center Hamburg-Eppendorf in compliance with German law (Tierschutzgesetz der Bundesrepublik Deutschland, TierSchG) and according to the guidelines of Directive 2010/63/EU. To obtain LSL-Cas9-Cre mice, the B6; 129-Gt(ROSA)26Sor$^{tm1(CAG-cas9*,-EGFP)Fezh}$/J (Jackson laboratory, Cat.: #024857)[71] mice were crossed with CMV-Cre-deleter mice.[72] The transgene-positive animals (heterozygous and homozygous) were identified based on the green fluorescence of the tail biopsies. C57BL/6J mice and LSL-Cas9-Cre were housed in C1ZMNHC1 Hamburg (Germany). Wistar rats were housed in the FTH of the UKE. All animals were housed at 22°C on a 12 h light/12 h dark cycle with *ad libitum* access to food and water in the breeding barriers of the Forschungstierhaltung of the University Medical Center Hamburg-Eppendorf. All experiments were approved by the local authorities of the State of Hamburg (Org 886; Nr.125/17). C57BL6J/UKE mice were used for mating and backcrossing.

Primary rat hippocampal and cortical cultures

Primary rat hippocampal cultures were prepared from Wistar rat embryos (E18) of both sexes. Rat dissociated hippocampal neurons were prepared like described in.[73] Briefly, hippocampi were collected in HBSS (Gibco, Cat.: #H9269-500ML) and digested for 15 min at 37°C in 0.025% Trypsin-EDTA (Thermo Fisher Scientific, Cat.: #25200-056). After multiple washing steps with DMEM (Gibco, Cat.: #H9269-500ML) supplemented with 10% FBS (Gibco, Cat.: # 10082147), 1% penicillin/streptomycin (Gibco, Cat.: #15140122), and 2 mM L-glutamine (Gibco, Cat.: #25030-024), the hippocampi were physically dissociated with needles and the density of neurons was determined by cell counting in a Neubauer chamber with Trypan Blue solution. Neurons were plated with a density of 60000 cells/ml onto poly-L-lysine-coated glass coverslips in BrainPhys (Stemcell Technologies, Cat.: #05790) supplemented with 1x SM1 (Stemcell Technologies, Cat.: #05711), and 2 mM L-glutamine (Gibco, Cat.: # 25030-024). For cortical cultures, cortex tissue was processed as described above, with the modified tissue dissociation step which was conducted with addition of 200 μg/mL of DNase I (Roche, Cat.: # 11284932001). The cortical neurons were plated with a density of 150000 cells/ml. Cells were kept at 37°C, 5% CO_2 and 95% humidity until use.

Primary mouse hippocampal cultures

Cultured mouse neurons were obtained from postnatal day 0 or 1 (P0-P1), transgene-positive LSL-Cas9-Cre mice of both sexes according to the previously published protocol.[73] Briefly, hippocampi were dissected from decapitated animals and collected in 450 μL HBSS (Gibco, Cat.: #H9269-500ML). 50 μL of Trypsin (0.25% Trypsin-EDTA, Thermo Fisher Scientific, Cat.: #25200-056) was added. Following the incubation at 37°C for 15 min, the tissue was washed with HBSS (Gibco, Cat.: #H9269-500ML), and the hippocampi were mechanically triturated in DMEM (Gibco, Cat.: #H9269-500ML) containing 10% FBS (Gibco, Gibco, Cat.: #10082147) and 0.5 mM L-glutamine (Gibco, Cat.: # 25030-024). Cells were plated onto 18 mm glass coverslips coated with poly-L-lysine at a density of 85000 cells/ml and grown in Neurobasal A (Gibco, Cat.: #12349015) supplemented with 1x B27 (Gibco, Cat.: # 17504044), 4 mM GlutaMax (Gibco, Cat.: # 35050087) and 1 mM sodium pyruvate (Gibco, Cat.: # 11360088). Cells were kept at 37°C, 5% CO_2 and 95% humidity until use.

Rat organotypic hippocampal cultures (OHSC)

The cultures were prepared from P5-P7 Wistar rats of both sexes. OHSC were prepared as described previously.[74] 400 μm thick slices were kept on porous membranes (Milicell CM, Millipore) in an incubator at 37°C, 5% CO2, 95% humidity with the antibiotics-free medium based on Minimal Essential Medium (Sigma, Cat.: #M7278) containing 20% heat inactivated horse serum (Sigma, Cat.: #H1138), 1 mM L-glutamine (Gibco, Cat.: # 25030-024), 0.01 mg mL−1 insulin (Sigma, Cat.: #I6634), 1.45 mL 5 M NaCl (Sigma, Cat.: #S5150), 2 mM MgSO4 (Fluka, Cat.: #63126), 1.44 mM CaCl2 (Fluka, Cat.: #21114), 0.00125% ascorbic acid (Fluka, Cat.: #11140), 13 mM D-glucose (Fluka, Cat.: #49152). Every 3rd day the 700 μL of the medium was exchanged.

Cell lines

Human embryonic kidney 293T (HEK293T) cells (ATCC, Cat.: #CRL-3216) and COS-7 cells (ATCC, Cat.: #CRL-1651) were maintained DMEM medium (Gibco, Thermo Fisher Scientific) supplemented with 10% FCS, 1x penicillin/streptomycin, and 2 mM L-glutamine at the 37°C, 5% CO_2, 95% humidity.

METHOD DETAILS

Antibodies

The following commercial primary antibodies were used in this study: mouse anti-LAMP1 (LY1C6, immunofluorescence, IF 1:500), rat anti-LAMP2 (GL2A7; IF 1:200), mouse anti-GAPDH (dot blot 1:1000) from Thermo Fisher Scientific; mouse anti-LAMP2 (H4B4; WB 1:1000) from Santa Cruz biotechnology; rabbit anti-GluN2B (IF 1:200) from Alomone Labs; guinea pig anti-Shank3 (IF 1:500) guinea pig anti-SAP102 (IF 1:500), rabbit anti-SAP102 (IF 1:500), guinea pig anti-MAP2 (IF 1:500), guinea pig anti-LAMP2A (IF 1:500), mouse anti-Hsc70 (IF 1:500), mouse anti-synaptotagmin1 Oyster650 (IF 1:200) from Synaptic Systems; mouse anti-Bassoon (SAP7F407) from Enzo; rabbit anti-tRFP (WB 1:1000) from Evrogen; mouse anti-GFP (B34, WB 1:1000) from BioLegend; rabbit anti-TDP-43 (IF 1:500) from Proteintech; rabbit anti-RFP (IF 1:500) from Rockland; rabbit anti-Huntingtin (Htt) (dot blot 1:1000), Rabbit anti-α-synuclein (D37A6) (dot blot 1:1000) from Cell Signaling Technology; Anti-GFP FluoTag-X4 (1:300), anti-GFP FluoTag-Q (1:300) from Nanotag Biotechnologies. Secondary antibodies used for IF (1:750): anti-mouse Alexa Fluor 568, anti-mouse Alexa Fluor 647, anti-rabbit Alexa Fluor 488, anti-rabbit Alexa Fluor 568, anti-rabbit Alexa Fluor 647, anti-guinea pig Alexa Fluor 488, anti-guinea pig Alexa Fluor 568, anti-guinea pig Alexa Fluor 647 from Thermo Fisher Scientific; anti-guinea pig Alexa Fluor 405 from Abcam; anti-mouse abberior STAR 635P, anti-rat abberior STAR RED, anti-rabbit aberrior STAR RED from Aberrior; anti-mouse Alexa Fluor 594, anti-rabbit Alexa Fluor 594, anti-guinea pig Alexa Fluor 594 from Antibodies online. Secondary antibodies used for WB (1:10000): anti-rabbit-IgG-HRP, anti-mouse-IgG-HRP from Dianova.

Biochemistry

Recombinant protein production

His-SUMO and His-SUMO-LAMP2B-404–415 were expressed in E. coli BL21 (DE3), induced with 400 μM isopropyl-beta-D-thiogalactoside (IPTG) followed by incubation at 25°C for 4 h. After lysis with lysis buffer (50 mM NaH2PO4, 300 mM NaCl, 10 mM imidazole, pH 8.0, EDTA-free protease inhibitor and PhosSTOP), the lysate was centrifuged at 20000 x g for 15 min. Supernatant was loaded on Ni-NTA resin and washed with wash buffer (50 mM NaH2PO4, 300 mM NaCl, 20 mM imidazole, pH 8.0). To check the purity and to quantify of the protein amount immobilized on bead, His-SUMO, His-SUMO-LAMP2B-404–415 and His-SUMO-LAMP2A-404–415 were resolved using 15–18% SDS-PAGE gels stained with Coomassie blue staining.

Pull-down assay

GFP-SAP102-PDZ1-3 and GFP-SAP102 SH3-GK were expressed in COS-7 cells (ATCC, Cat.: #CRL-1651) and lysed in lysis buffer (50 mM HEPES pH 7.0, 100 mM NaCl, 1% Triton X-100, EDTA-free protease inhibitor and PhosSTOP (Roche, Cat. #04906837001)). The lysate was incubated at 4°C for 1 h rotating followed by a brief sonication and centrifugation for 10 min at 12000 x g and the supernatant was collected.

Pull-down assays were used to assess the direct interaction between LAMP2B-404–415 or His-SUMO-LAMP2A-404–415 with GFP-SAP102-PDZ1-3 and GFP-SAP102-SH3-GK. Briefly, 5 μg of His-SUMO-LAMP2B-404–415/-LAMP2A-404–415 along with the equivalent amount of the control protein His-SUMO bound on the beads was incubated with COS-7 cell lysate overnight at 4°C on a rotary shaker. After three washing steps with wash buffer (50 mM NaH_2PO_4, 300 mM NaCl, 20 mM imidazole, pH 8.0, 1% Triton X-100, EDTA-free protease inhibitor and PhosSTOP) the complex was eluted in 2x SDS sample buffer and subjected to Western blot. In a competitive pull-down, 10 μg of TAT-Scr or TAT-LAMP2B-404–415 peptide was incubated along with COS-7 cell lysate.

Heterologous co-immunoprecipitation (Co-IP)

The constructs pEGFP-N1 (Clontech, Cat.: #6085-1), pEGFP-GluN2B-840–1482, ptRFP-LAMP2B, and pmCherry-Jacob were heterologously expressed in HEK293T cells. The cells were transfected with PEI when the confluency reached 50–60%. The DNA was mixed with MaxPEI (Polysciences, Cat.: #23966) in a ratio of 1:3 (DNA:PEI) in DMEM medium without supplements and incubated for 20 min at RT. The DNA-PEI-mixture was added to the cells and the collected medium was replaced after 4 h of incubation. Transfected HEK293T cells were lysed in RIPA buffer (50 mM Tris-HCl pH 8.0, 150 mM NaCl, 1% Triton X-100, 0.5% sodium deoxycholate, 0.1% SDS, EDTA-free protease inhibitor and PhosSTOP) for 1.5 h rotating at 4°C. The lysate was centrifuged at 20000 x g for 20 min at 4°C and supernatant was incubated with anti-GFP-coated magnetic beads (MultiMACS GFP Isolation Kit, Miltenyi Biotec, Cat. #130-094-253). The co-immunoprecipitation was carried out according to the manufacturer's protocol.

Dot blot

DIV16-21 cortical neurons were treated with 20 μM of NMDA (Sigma Aldrich, Cat.: #M3262) for 15 min. For some experiments, neurons were pre-treated over night with 2.5 μM of TAT-Scr or TAT-LAMP2B-404–415 peptide. The culture medium was collected and concentrated 20 x using Amicon Ultra-0.5 Centrifugal Filter Unit (3 kDa cut off). A nitrocellulose membrane was placed over the blotting membrane onto a 96-well Bio-Dot SF Microfiltration Apparatus (Biorad) and pre-soaked in Tris-buffered saline (TBS buffer; 20 mM Tris, 150 mM NaCl, pH 7.4) under the vacuum manifold base. 5 μL media were blotted onto the membrane. The membrane

was removed and the membrane was dried for 1 h. Blocking of the membrane was performed with 5% BSA in Tris-buffered saline/Tween (TBS-T, 20 mM Tris, 150 mM NaCl, pH 7.4, 0.1% Tween 20) buffer for 1 h, followed by incubation of primary antibody overnight.

Enzyme-linked immunosorbent assays (ELISA)

For viral infections of cortical cultures, adeno-associated virus of serotype 9 (AAV9) encoding.

GFP or TDP-43-GFP was produced by the Hamburg Center for Experimental Therapy Research (HEXT) Vector Core Unit, University Medical Center Hamburg-Eppendorf, Hamburg, Germany. 2*10^{10}GC/well were added to the DIV7 cells. After 7 days, the coverslips were flipped on Tyrode's buffer (128 mM NaCl, 5 mM KCl, 1 mM $MgCl_2$, 2 mM $CaCl_2$, 4.2 mM $NaHCO_3$, 20 mM glucose, and 15 mM HEPES; pH = 7.2–7.4) for stimulation. Then, the buffer was collected and centrifuged at 1500 rpm for 10 min at 4°C. For detection, a GFP ELISA kit (Abcam, Cat. # ab171581) was used according to the manufacturer's instructions.

Immunostaining and microscopy

Cell based co-recruitment assay

HEK293T cells were transfected with the following constructs: pEGFP-SAP102-SH3-GK or pEGFP-SAP102-PDZ1-3 with pGolt-mCherry-LAMP2B-404–415, pGolt-mCherry-GluN2B-840–11482 or empty pGolt-mCherry. On the following day, cells were fixed with 4% PFA, permeabilized with 0.1% TX-100 in 1xPBS for 10 min, stained with 4′,6-diamidino-2-phenylindole (DAPI; Vectashield/Biozol, Cat. #BCL-BCFA-211) and mounted in Mowiol 4–88 (Merck Chemicals; Cat. #4375904). The z stack images were acquired with Leica TCS SP5 system controlled by Leica LAS AF software, with 300 nm with step size was taken with 512 × 512 pixels format. Maximal intensity images from three optical sections were generated for representative images.

OHSC stimulation and imaging

The DIV7-10 slices were electroporated with the SEP-LAMP2 and mCerulean and expressed for 5–8 days. For imaging, the slices were placed into the chamber containing HEPES buffer (145 mM NaCl, 10 mM HEPES, 25 mM $C_5H_{12}O_6$, 2.5 mM KCl, 1 mM $MgCl_2$, 2 mM $CaCl_2$; pH 7.4, 318 mOsm) at 27°C–29°C. Imaging was performed in a custom-built two-photon laser scanning microscope based on an Olympus BX51WI microscope. Images were acquired with WPlan-Apochromat 40×/1.0 NA (Zeiss) objective and controlled by ScanImage 2017b (Vidrio). A Ti:Sapphire laser (Chameleon Ultra, Coherent) controlled by an electro-optic modulator (350-80, Conoptics) was used to image mCerulean volume fill at 820 nm and SEP at 980 nm. The images were acquired at 1.48 Hz. At the beginning, a z stack with 500 nm step size was acquired for the mCerulean channel. Subsequently one focal plane was selected and following baseline acquisition 50 μM picrotoxin (PTX, Merck Milipore, Cat. #528105) or DMSO (vehicle control, Sigma Aldrich) diluted in HEPES buffer was perfused. For GluN2B inhibition slices were pre-incubated with 5 μM ifenprodil hemitartrate (Tocris, Cat.#0545) for 60 min and throughout the recording. At the end, additional z stack with 500 nm step size was acquired for the mCerulean channel 30–45 min post stimulation.

Primary cultures transfection and stimulation

Primary hippocampal neurons were transfected with Lipofectamine 2000 according to the protocol provided by the supplier (Invitrogen/Thermo Fisher Scientific). For LAMP1 knockdown experiments, DIV7 neurons were transfected with LAMP1 shRNA (5′-CCAGTGTGTCCAAGTACAA-3′) or scrambled control (5′ GGATGAGTCCTCCATGTTCT-3′)[75] and kept for 5 days. For CRISPR/Cas9-mediated gene downregulation experiments, DIV7 mouse hippocampal neurons were transfected with constructs encoding GluN2B gRNA1 (5′-GTTGGCCGTCTTGGCCGTAT-3′) and gRNA2 (5′-GTGTTCGGACAGCATGTCCG-3′) or SAP102 gRNA (5′-GGCCCTGTTTGATTATGAT-3′) for 5–7 days.

All experiments were conducted with mature neurons (DIV >15). The overexpression of LAMP1, LAMP2B, GluN2B, or KFERQ fusion proteins or TREMARCKS-GFP-H1[76] was for 1 day. For stimulation 20 μM of NMDA (Sigma Aldrich, Cat.: #M3262) was applied to the bath for 15 min. Neurons were incubated over night with 20 μM of the CMA activator CA77.1 (MedChemExpress, Cat. #HY-134923) or for 20 min with 20 μM of CMA inhibitor 17-Dimethylaminoethylamino-17-demethoxygeldanamycin (17-DMAG; Merck, Cat.: #D5193). For GluN2B inhibition slices were pre-incubated with 5 μM ifenprodil hemitartrate (Tocris, Cat.#0545) for 60 min and throughout the recording.

Immunofluorescence (IF)

The cells were fixed in 4% PFA with 4% sucrose for 15 min at RT, washed with PBS and permeabilized in 0.2% Triton X-100 in PBS for 10 min. After incubation in blocking solution (2% glycine, 2% BSA, 0.2% gelatine and 50 mM NH_4Cl in PBS) for 1h at RT, the primary antibody diluted in blocking solution was incubated over night at 4°C. The cells were washed in PBS, incubated for 1 h with secondary antibody in blocking solution at RT and, after additional PBS washes, mounted in Mowiol 4–88 (Merck Chemicals; Cat. #4375904).

GluN2B surface staining was performed for 10 min at RT in Tyrode's buffer (128 mM NaCl, 5 mM KCl, 1 mM $MgCl_2$, 2 mM $CaCl_2$, 4.2 mM $NaHCO_3$, 20 mM glucose, and 15 mM HEPES; pH = 7.2–7.4) containing the rabbit anti-GluN2B antibody (Alomone Labs, Cat.: #AGC-003), following a wash with Tyrode's buffer and PFA fixation as described above.

For the surface staining with α-GFP-AF647 nanobody (Anti-GFP FluoTag-X4, Cat.: #N0304-Af-647-L) detecting different versions of GFP, including SEP, transfected neurons were incubated with 20 μM NMDA for 10 min, and for the last 5 min with 20 μM NMDA

(Sigma Aldrich, Cat.: #M3262) and nanobody dilution. Control group was incubated with nanobody only. All substances were diluted in the culture media. The cells were washed, fixed with PFA, and stained with respective antibodies as described above.

Confocal and STED microscopy

Images were acquired in a Leica TCS SP5 system controlled by Leica LAS AF software using HCX PL APO 63 ×/1.40 NA objective. Areas of 82 × 82 μM were scanned with 405, 488, 568 and 635 nm laser lanes (12-bits, 80 × 80 nm pixel size, 700 Hz, Z-step 0.3 μm). Fluorescent signal was collected using three HyD detectors.

Stimulated emission depletion (STED) images were acquired with an Abberior microscope controlled by Imspector software (Abberior Instruments). STED laser lines 561 and 640 nm were used for excitation while a 775 nm laser was used for depletion of fluorescence. Cells were imaged with a 60x NA = 1.4 P-Apo Oil objective from Nikon.

Live imaging experiments

Live cell imaging was performed using a Nikon Eclipse Ti-E controlled by VisiView software (Visitron Systems). The built-in Nikon perfect focus system kept the region of interest in fixed focal plane. 405, 488, 561 and 640 nm excitation lasers were used. Cells were imaged with a 100× (Nikon, CFI Plan Apochromat Lambda 100×/1.45 NA) objective equipped with 2x Photometrics Prime 95B camera. TIRFM images were obtained with an iLAS2 (Gattaca systems) spinning-TIRF system. The frequency of acquisition varied depending on the experiments and is indicated below. All experiments were performed in Tyrode's buffer at 37°C and 5% CO_2, with the exception of lysosomal de-acidification experiment where Tyrode's buffer containing 50 mM NH_4Cl was used. To label active lysosomes the cells were pre-incubated with 0.5% Magic Red (Bio-Rad, Cat.: #ICT937) for 30–60 min, 10 nM BODIPY FL-pepstatin A (Thermo Fischer Scientific, Cat.: #P12271) for 30–90 min or 0.5 μM SiR-lysosome (Spirochrome, Cat.: #SC012) for 60–120 min.

For lysosomal stalling assay, the images were acquired at 0.5 Hz frequency for 15–16 min 20 μM NMDA was applied after 20–40 frames of baseline acquisition. 2.5 μM of TAT-Scr or TAT-LAMP2B-404–415 peptide was applied overnight and present throughout the time of imaging.

For lysosomal fusion experiments, neurons were electrically stimulated with 2 electrodes placed at the edges of coverslip with 900 pulses at 20 Hz (Warner Instruments),[73] in the presence of 0.1 μM Bafilomycin A1 to avoid signal re-acidification.[10] The images were acquired at 1 Hz. For NMDA-induced fusion, 20 μM NMDA was added to the bath following the baseline acquisition (4–6 frames). The images were acquired at 0.14 Hz or 0.25 Hz. For GluN2B inhibition, 5 μM ifenprodil was pre-incubated for 60–90 min 2.5 μM of TAT-Scr or TAT-LAMP2B-404–415 was applied overnight.

QUANTIFICATION AND STATISTICAL ANALYSIS

Colocalization analysis

Fiji[77] software was used for colocalization analysis. The regions of interest (ROIs) were created with the circular enlargement of local fluorescence intensity maxima or lasso tool. The overlap and direct apposition of segmented ROIs was collectively defined as association. The overlap was defined as colocalization.

For STED images deconvolution using the Imspector (Aberrior instruments) software was used applying the Richardson-Lucy algorithm with a number of iterations of 4. A 2D Gaussian function: $f(x, y) = a \exp(-x^2/2\sigma_x^2 + y^2/2\sigma_y^2)$. Full width half maximum set to 50 nm for σ_x/y = 50 nm/2ln2 was used as theoretical estimate of the system point spread function (PSF). The line profiles were created using the ''Plot profile'' tool of Fiji to measure the signal intensities along the defined line. The intensities were normalized to the maximum intensity value for individual channels. For colocalization experiment with at least one overexpressed protein (LAMP2B-GFP and Hsc70 or LAMP2B-GFP and TDP-43-tdTomato) the binary mask was applied on filtered LAMP2B-GFP channel (median filter). The positive signal from the other channel was identified with find maxima function. To estimate the specificity of co-localization over chance (i.e., random colocalization), the number of maxima within the LAMP2B-GFP mask normalized to total maxima was divided by the number of maxima rotated by 180° within the same LAMP2B-GFP mask. The Pearson's correlation coefficient was calculated on cropped deconvolved images with the Imaris (Bitplane) colocalization tool. To estimate chance colocalization, the image of one channel was rotated by 180°.

Immunofluorescence intensity quantification

For analysis of the surface staining with α-SEP-AF647 nanobody, the mean fluorescence intensity was measured within each dendritic stretch and normalized to the averaged fluorescence intensity of the control group. For the association studies only dendritic stretches with mean fluorescence intensity above the control group were analyzed.

For the evaluation of shRNA-mediated knockdown and CRISPR/Cas9-mediated gene downregulation, only transgene-positive neurons characterized by pronounced green fluorescence were analyzed. The mean fluorescence intensity of the averaged projection of three focal planes was quantified in somatic and dendritic regions. The values were normalized to the mean fluorescence intensity of the control group.

Lysosomal fusion analysis

When necessary, image streams were stabilized using template matching plugin (Fiji). The fusion events were identified based on the following equation: $\Delta F = \frac{(F - F_{baseline})}{F_{baseline}} * 100$ where $F_{baseline}$ equals averaged fluorescence intensity of baseline, and F equals fluorescence intensity of the given frame. The fluorescence was measured within circular ROIs of 0.77 μM diameter. The fusion event was defined as increase of fluorescence in the last 20 frames greater than 1.5 multiplication of baseline standard deviation. Only the ROIs with stable baseline (i.e., R^2 value of logarithmic fit below 0.3) were taken into account. For the fusion density calculation, the number of identified fusion ROIs was divided by the length of the dendritic stretch. For the fusion intensity quantification, the averaged fluorescence increase of the last 20 frames from ROIs identified within one dendritic stretch was calculated. The fusion curves were generated by plotting averaged fluorescence intensity of dendritic stretch at the given time point, the shading indicates ±SEM. The representative images were created by subtracting the averaged baseline image from each frame of the stream. The noise (measured within ROI outside of the transfected cell) was subtracted with math function equally for each pixel from the averaged baseline and last 20 frames, and the resulting image was filtered with median function.

Dendritic spine analysis

Dendritic spines were analyzed according to Wiegert et al.[78] Briefly, maximum intensity projections of 3 focal planes before and 30–45 min after perfusion were created. For estimating the z position of 2D image time series with respect to a 3D reference stack custom python code was used (python version 3.8). Individual images from the time series were placed in a dummy 3D stack and the positional offset was calculated using phase cross correlation (scikit-image.org) after smoothing (Gaussian filter, sigma = 1.0) and thresholding (Otsu method). The fluorescence intensity of every detected spine head was normalized to the averaged fluorescence of the dendritic shaft (maximal fluorescence intensity). The change in the spine volume was calculated according to the equation $\Delta volume = \frac{(normalized\ F_{after} - normalized\ F_{before})}{normalized\ F_{before}} * 100$ and the distance to the closest identified fusion spot was measured. To compare the effect of fusion on structural plasticity, the change in dendritic spine volume within the 5 μm radius from the fusion event was compared to randomly assigned ROIs in dendritic shaft of dendrites from slices stimulated with DMSO where no fusion was detected.

Analysis of trafficking

When necessary, image streams were stabilized using template matching plugin and bleach-correction was applied (Fiji). To quantify vesicular kinetics, the kymographs were created with Multi Kymograph function (Fiji) and the velocity was measured using the Velocity Measurement Tool. The beginning and the end velocity was measured within the first and last third of the stream respectively.

To analyze co-trafficking and directionality of movement, the kymographs were created using the KymographClear[79] or the Multi Kymograph plugin of Fiji. Dendritic stretches were traced using the segmented line tool. Line thickness was chosen between 3 and 5 pixels depending on the thickness of the dendrite. In experiments with two or more channels imaged simultaneously, overlapping traces were counted as co-trafficking.

To quantify the relation between LAMP2B-mKate or Magic Red and SEP-GluN2B the colocalization between ROIs identified on the first 5 frames was quantified as described above, with 0.77 μm ROIs diameter. The transient association was assumed for colocalization duration of at last 5 s.

Figure preparation and statistical analysis

All image analysis was performed on the raw data. All analysis was performed by a researcher blind to experimental groups (treatments, transfected constructs). The cells displaying abnormal morphology or protein localization (i.e., aggregates in the soma, lack of initial mobility for vesicular proteins) were classified as overexpression artifacts and excluded from the study.

For some representative images, linear contrast adjustment (histogram normalization), background subtraction, median and Gaussian filters were applied (equally to all representative images within experiment).

Data are shown in the manuscript as mean ± SEM and n-numbers used for statistics are indicated in each panel of the figure. Statistical analysis was carried out using GraphPad Prism (GraphPad Software). Grubb's outlier test $\alpha = 0.05$ was applied. Next, D'Agostino and Pearson normality test was performed to assess the data distribution. Significance was assessed by parametric or non-parametric tests, accordingly. For parametric data, two-tailed unpaired Student's t-test or one-way ANOVA with Tukey posthoc test for multiple comparisons was used. For two-parameter analysis two-way ANOVA with Tukey posthoc test for multiple comparisons was used. For not normally distributed data, Mann-Whitney *U* test was used to compare two groups or Kruskal-Wallis test for multiple comparisons. P-values were considered as following: $p > 0.05$ = ns; ≤ 0.05 = *; ≤ 0.01 = **; ≤ 0.001 = ***; ≤ 0.0001 = ****. The type of statistical test used for each experiment, significance levels, the n number definition, and the look-up table (LUT) are reported in the corresponding figure legends.